NASA TECHNICAL NOTE

NASA TN D-6269

NASA TN D-6269

AERODYNAMIC CHARACTERISTICS OF A LARGE-ANGLE BLUNT CONE WITH AND WITHOUT FENCE-TYPE AFTERBODIES

by Kenneth W. McAlister, David A. Stewart, and Victor L. Peterson

Ames Research Center
and
U.S. Army Air Mobility R&D Laboratory
Moffett Field, Calif. 94035

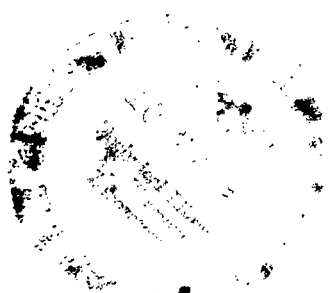

NATIONAL AERONAUTICS AND SPACE ADMINISTRATION • WASHINGTON, D. C. • APRIL 1971

1. Report No.	2. Government Accession No.	3. Recipient's Catalog No.
NASA TN D-6269		

4. Title and Subtitle

AERODYNAMIC CHARACTERISTICS OF A LARGE-ANGLE BLUNT CONE WITH AND WITHOUT FENCE-TYPE AFTERBODIES

5. Report Date: April 1971

6. Performing Organization Code:

7. Author(s): Kenneth W. McAlister, David A. Stewart, and Victor L. Peterson

8. Performing Organization Report No.: A-3845

9. Performing Organization Name and Address:
NASA Ames Research Center
and
U.S. Army Air Mobility R&D Laboratory
Moffett Field, Calif., 94035

10. Work Unit No.: 120-05-02-02-00-21

11. Contract or Grant No.:

12. Sponsoring Agency Name and Address:
National Aeronautics and Space Administration
Washington, D. C., 20546

13. Type of Report and Period Covered: Technical Note

14. Sponsoring Agency Code:

15. Supplementary Notes:

16. Abstract

Hypersonic experiments on sting-mounted and free-flying models were conducted to show that the base-forward stable trim point of a large-angle blunt cone can be eliminated by adding a fence-type afterbody. Several configurations were investigated in detail and it is shown that the fence must be symmetric, have a sharp trailing edge, and provide sufficient flow relief near the base of the cone. Transonic dynamic stability characteristics were also obtained from tests of free-flying models. Finally, all test results were synthesized into a continuous description of the aerodynamic characteristics for use in trajectory calculations. It was found that for a 1 rad/s rolling entry into the Earth's atmosphere the vehicle would be properly oriented in nose-forward flight well before peak heating, even when entering with a nearly base-forward attitude.

17. Key Words (Suggested by Author(s))
Blunt body
Cone
Reentry capsule
Destabilizing afterbody

18. Distribution Statement
Unclassified–Unlimited

19. Security Classif. (of this report)	20. Security Classif. (of this page)	21. No. of Pages	22. Price*
Unclassified	Unclassified	49	$3.00

*For sale by the National Technical Information Service, Springfield, Virginia 22151

SYMBOLS

C_A	axial-force coefficient, $\frac{\text{axial force}}{qS}$
C_D	drag coefficient, $\frac{\text{drag}}{qS}$
C_L	lift coefficient, $\frac{\text{lift}}{qS}$
C_{L_α}	lift-curve slope
C_m	pitching-moment coefficient, $\frac{\text{pitching moment}}{qSd}$
$C_{m_{\alpha_l}}$	quasi-linear value of pitching-moment-curve slope
$C_{m_q} + C_{m_{\dot{\alpha}}}$	damping-in-pitch derivative, $\frac{\partial C_m}{\partial(qd/V)} + \frac{\partial C_m}{\partial(\dot{\alpha}d/V)}$
C_N	normal-force coefficient, $\frac{\text{normal force}}{qS}$
C_p	pressure coefficient
d	maximum diameter of model
I	moment of inertia with respect to the pitch axis
M	Mach number
m	mass of model
q	free-stream dynamic pressure
r	radius
R	base radius of model (maximum)
Re	Reynolds number (based on model diameter and free-stream air properties)
S	base area of model
t	time
V	velocity of the model with respect to still air

x	displacement in positive drag direction
x_{cg}	distance from model nose to center of gravity
y	displacement in positive lift direction
α	resultant angle of attack (zero with nose windward)
$\dot{\alpha}$	angular rate
α_m	average value of maximum resultant angle-of-attack envelope
α_{rms}	root-mean-square resultant angle of attack (integrated over trajectory)
β	angle of yaw
θ	pitch angle
λ	wavelength of model oscillation
ξ	dynamic stability parameter, $C_D - C_{L_\alpha} + (C_{m_q} + C_{m_{\dot{\alpha}}})(d/\sigma)^2$
ρ	gas density
σ	radius of gyration with respect to the pitch axis, $\sqrt{I/m}$

AERODYNAMIC CHARACTERISTICS OF A LARGE–ANGLE BLUNT CONE WITH AND WITHOUT FENCE–TYPE AFTERBODIES

Kenneth W. McAlister, David A. Stewart, and Victor L. Peterson

Ames Research Center
and
U.S. Army Air Mobility R&D Laboratory

SUMMARY

The possibility of eliminating base-forward aerodynamic stability of a spherically blunted 60° half-angle cone at hypersonic speeds was investigated by adding fence-type afterbodies. These tests involved free-flying models in the Ames combustion driven 42-Inch Shock Tunnel at Mach number 12.5, and sting-mounted models in the Ames 3.5-Foot Hypersonic Wind Tunnel at Mach number 10.4. Free-flying models were also tested in the Ames Pressurized Ballistic Range to determine nose-forward dynamic stability at transonic speeds.

Results of these tests showed that it is possible to eliminate base-forward stability by adding a fence-type afterbody. It was found that the fence should be vented and symmetric, and have a sharp trailing edge in order to provide the necessary overturning moment. Pressure measurements over the base of the model indicate that this moment is not due to the fence altering the pressure distribution on the base but to aerodynamic forces on the fence itself.

Models having a cylindroconical fence were tested at transonic speeds and shown to be statically stable and dynamically unstable at all Mach numbers and throughout the angle-of-attack range of the investigation.

A trajectory analysis of the results of each test showed that while rolling 1 rad/s the vehicle could enter the Earth's atmosphere in a nearly base-forward attitude and still become oriented nose-forward well before peak heating occurred. The variation in angle-of-attack envelope, however, was not monotonic over the entire trajectory and large amplitudes may recur during the transonic flight regime.

INTRODUCTION

Advanced space-power systems capable of providing large amounts of electric power are now under study. One of these systems converts heat produced by radioactive decay into electric energy through an intermediate mechanical process based upon the Brayton cycle. It was envisioned that this radioactive material would be suitably contained and then launched into space where part of the container would also function as a heat exchange surface in the Brayton cycle. This container would furthermore act as a vehicle when the radioactive material is returned from space. A principal concern in the development of this nuclear fueled power system is the potential radiation hazard

not only before and during actual use, but also in connection with its disposal. The problem of safety places unusual constraints on the design of the vehicle carrying the radioactive material. To be as failure proof as possible, the vehicle, initially having an arbitrary attitude, must be capable of surviving an uncontrolled reentry into the Earth's atmosphere.

The entry-vehicle shape that evolved during the preliminary design study (ref. 1) is a 60° half-angle blunted cone in which capsules containing Pu 238 fuel are arranged in a circular planar array lying almost in the base plane of the vehicle. The flat base of the vehicle which forms the heat exchange surface was a design requirement, but was recognized as an undesirable shape from an aerodynamic standpoint. Such a vehicle could fly stably either nose forward or base forward, depending upon its attitude at the beginning of atmosphere entry. Of course, base-forward flight is unacceptable since the exposed capsules containing the radioactive material would then be subjected to severe aerodynamic heating. An earlier study (ref. 2) showed that relatively short blunt-nosed bodies of revolution can be made to fly in the preferred nose-forward attitude by adding either a conically or spherically shaped afterbody of proper dimensions to position the center of pressure aft of the mass center when the body is in the base-forward attitude. The tactic of eliminating base-forward stability by enclosing the vehicle base with a full afterbody cannot be used in the present situation, however, since a large portion of the inner part of the base area must be exposed to permit radiative heat exchange.

Several concepts involving the use of asymmetric aerodynamic fence-type afterbodies had been proposed for eliminating base-forward aerodynamic stability; however, preliminary tests in the Ames 42-Inch Shock Tunnel showed these fences to be aerodynamically ineffective. Therefore, an experimental investigation was undertaken to find an effective fence. From this study two basic symmetric fences developed which appeared to meet the criteria outlined in reference 1. Detailed experiments were then made with sting-mounted models in the Ames 3.5-Foot Hypersonic Wind Tunnel. Since configurations of this general type have been found to be dynamically unstable at transonic Mach numbers (ref. 3), free-flight tests were also made in the Ames Pressurized Ballistic Range.

EXPERIMENTS

The various fence geometries to be discussed in the following sections are summarized in table 1 and figure 1.

Hypersonic Tests of Free-Flying Models

Models- The model assembly consisted of an extruded lucite forebody, a nylon base and afterbody, and a cylinder of tungsten alloy located on the geometric axis. Three asymmetric fences (fig. 1) having flare angles of 0°, -16.7°, and -30.0° were tested with a 10.2-cm (4 in.) diameter model. Two positive-flare symmetric fences, conical and cylindroconical, were tested with a 12.7-cm (5 in.) diameter model. The trailing-edge thickness of these fences was approximately 0.025 R. The tungsten alloy cylinder was suitably dimensioned to locate the center of gravity at 0.54 R from the nose for the asymmetric fence models, and 0.64 R for the symmetric fence models.

Facility and test conditions- The hypersonic free-flight tests were performed in the Ames 42-Inch Shock Tunnel (combustion driven) with air as the test gas. The facility was operated in the tailored-interface mode to provide a reservoir pressure of 286 atm and an enthalpy of 9.3 MJ/kg (4000 Btu/lb_m). The air was expanded through a 10° half-angle conical nozzle to generate a 4130 m/s flow at a Mach number of 12.5. The Reynolds number was 19,500 based on model diameter and corresponds to an altitude of 53.7 km (176,000 ft) based on density. The duration of each test was nominally 20 ms. The calibration of this facility is discussed in detail in references 4 and 5. The models were suspended at various initial angles of attack in the test section by a pair of 10 μm (0.4 mil) nylon threads. These threads were attached to adjustable overhead supports to permit proper positioning of the model in the test section. At the start of the high-temperature flow the threads were vaporized and the model was released in free flight. The blockage factor for the largest model was 1.4 percent. Figure 2 shows a conical fence model suspended by threads in the 42-inch test section prior to flow development.

Data acquisition and reduction- The plane of motion was established by the initial model orientation in the test section. The model flight could therefore be adequately defined from analysis of motion pictures recorded by a single 16-mm camera. A grid located on the opposing test section wall (fig. 2) provided a reference from which linear and angular displacements could be determined. The time measure was taken from the fixed exposure rate of 500 frames per second. The accuracy of this rate was monitored by exposing the film strip to a precision 120 cps chopped light source. Representative enlarged motion picture frames from two tests are given in figure 3. The model was typically displaced a distance of 9-cm longitudinally during the period of established flow. The dynamic pressure for each test was inferred from the simultaneous displacement of a 2.54 cm diameter sphere. The estimated maximum error in dynamic pressure obtained in this manner was ±5 percent.

The translational and angular displacements defining the planar motion were read from the filmed flight and approximated by a polynomial function of time. The free-flight displacements from a selected test are presented as an example in figure 4. Measurement accuracies were nominally x ±0.9 mm, y ±0.5 mm, and θ ±0.002 rad. A fifth-degree polynomial was generally found to represent the discrete points of data to within 1 percent. The pitch moment of inertia of each model was measured prior to flight to an accuracy of ±2 percent. These measurements and the second derivatives of the displacement expressions were used to obtain lift, drag, and moment coefficients from the governing momentum equations.

Hypersonic Tests of Sting-Mounted Models

Models- Models having a base diameter of 20.3 cm (8 in.) were cast from 309 corrosion-resistant steel. The interchangeable afterbodies were either vented conical, cylindroconical (also unvented), or extended fence-type configurations. The conical fence was flared 14° and had a trailing-edge thickness of 0.047R. The conical portion of the cylindroconical and extended fences was flared 36.6° and had a trailing-edge thickness of 0.031R. The trailing edges of these fences were later sharpened (to radius of about 0.0005R), and the flare-angle consequently increased; however, the maximum diameters were held equal and fixed. The angle between the sting and model axes could be varied from 0° to 180° in 15° increments, enabling measurements to be obtained throughout the complete angle-of-attack range. A special plate containing a polar array of 50 orifices (fig. 5) was used to obtain base-pressure measurements. Each orifice had a diameter of 0.107 cm.

Facility and test conditions- Tests were conducted in the Ames 3.5-Foot Hypersonic Wind Tunnel in heated air with an injected helium boundary layer as a thermal buffer. Each model was inserted in the stream after tunnel flow was established and withdrawn before the flow was terminated. The strut was translated to maintain the model near the center of the flow core during angular displacements to 20°. The 15° model-to-sting angle intervals coupled with the continuously variable 20° strut angle range permitted the complete angle-of-attack range to be surveyed with some data overlap. The blockage factor (based on the maximum projected area ratio) relative to the test section was 3.6 percent. Each run permitted a nominal testing time of 90 seconds under conditions of 54-atm total pressure and 1110° K (2000° R) total temperature at a Mach number of 10.4. The Reynolds number was about 1×10^6 based on model diameter. At a higher density shadowgraphs were also obtained at a Mach number of 7.4 under conditions of 17-atm total pressure and 720° K (1300° R) total temperature. The Reynolds number at this lower Mach number was on the order of 1.2×10^6. Figure 6 shows a sting-mounted model (with cylindroconical fence) at zero angle of attack in the 3.5-foot wind tunnel.

Data acquisition and reduction- Forces and moments were measured with a six-component strain-gage balance having limits of 890 N (200 lb_f) and 22.6 m·N (200 in.-lb_f). The balance temperature was maintained at 339° K (150° F) by water circulating through a surrounding jacket with metal bellows connections. The balance was calibrated at this temperature to an accuracy of 1 percent of full-scale. The pressure distribution over the base of the model was measured by 0.34 atm absolute transducers mounted in a cell block outside the test section. Each base-plate orifice was connected to an individual pressure cell by a 1.8-m length of 1.6-mm (1/16 in.) tubing.

The transducer outputs at each model attitude during a run were sampled at intervals giving 10 groups of 3-cycle data. This schedule resulted in a cycle period of 0.02 s and a sampling period of 1.0 s. These data were passed through an analog-digital converter and recorded on magnetic tape, from which test conditions, force, moment, and pressure coefficients were computed. Model base diameter and area were selected as reference scales for the aerodynamic coefficients. The moment center was taken to be 0.61R from the nose. During each instrumented test, the continuous outputs from selected transducers were monitored on an oscillograph to detect possible mechanical interference, flow instability, weak-strong shock transition on the model, and the onset of flow breakdown. Impact pressure was also measured at various locations near the model-sting intersection to assess the wake disturbance due to the sting and strut. This disturbance was found to be within the accuracy of the balance measurements and was therefore neglected.

Transonic Tests of Free-Flying Models

Models- Each model had a cylindroconical fence and was machined as a complete unit from a tungsten-base alloy having a density of about 17 g/cm^3. A portion of the model interior was removed, locating the center of gravity at 0.56R from the nose. Close dimensional tolerances gave maximum mean deviations between models of 0.5 percent for mass, 0.9 percent for pitch moment of inertia, and 0.4 percent for the center-of-gravity location. Exact measures are given in table 2. Two small pins (one sharpened for distinction) were located on the trailing edge of the fence to facilitate the detection of any unintentional roll imparted to the model upon launch.

Facility and test conditions- For the transonic tests in the Ames Pressurized Ballistic Range models were launched from a smoothbore 57-mm powder gun into still air at ambient conditions. The test section consists of a closed vessel, 62 m in length, along which 24 shadowgraph stations are located. The minimum model-to-test gas density ratio was established by an anticipated value for C_{m_α}, a desired pitching wavelength of 17 m, the known dimensionless moment of inertia, and the existing gun bore. The test gas density, as given by the following equation (hence the test Reynolds number), was therefore limited by available material densities.

$$\rho = \frac{8\pi^2 I}{C_{m_\alpha} S d \lambda^2}$$

It was determined that a 5.0-cm model machined from the high-density tungsten-base alloy material would allow a test Reynolds number of about 1×10^6 to be obtained. Limited to ambient temperature air, this model density therefore required the test pressure to be 1 atmosphere. The blockage factor in this facility was 0.03 percent.

The launch sabot was machined from nylon and consisted of a pusherplug for thrust transmission and four peripheral guides to center the model securely on the gun axis. The five-piece sabot, which was intended to carry the model at zero angle of attack, is shown partially assembled with the model in figure 7. The leading edges of the sabot guides were shaped such that the sabot would be aerodynamically stripped away from the model after clearing the muzzle. Because of the high pitching moment of inertia of the model, initial angles of attack resulting from the uneven parting of the sabot were usually below 10°. Larger initial angles were obtained by partially blocking the model path early in flight with a section of dense foam rubber about 5 cm thick. The impulse resulting from this impact at a Mach number of 1.2 was found to give the model an initial angle of attack of over 30°.

Data acquisition and reduction- The flight history of each model was determined from digital chronographs (providing the time measure at known intervals) and orthogonal shadowgraphs (providing the relative translation and rotation measure). Mathematical functions fit to the smoothed discrete data points provided a continuous description of model motions. A cursory inspection of the oscillatory motion enabled the flight data to be segmented and analyzed over sections of nearly constant Mach number. The drag was obtained from time and distance measurements, the static- and dynamic-stability parameters from the oscillatory motion, and the lift-curve slope from the swerve. Details of this procedure are given in reference 7. Typical graphical displays of diverging motions in the θ - β plane (angles of pitch and yaw, respectively) are shown in figure 8. Both of these particular motion histories were segmented into five overlapping intervals (see stations in table 2), each having three consecutive peaks of resultant angle of attack.

RESULTS AND DISCUSSION

Hypersonic Aerodynamic Characteristics

Two types of fences designed to eliminate the base-forward aerodynamic stability of a 60° half-angle blunted cone were investigated. One type was asymmetric in that they extended only half way around the model base; the other type was symmetric and extended entirely around the model base (see fig. 1).

Results from exploratory tests of asymmetrically shaped fences (fig. 9) show that only the -30° fence produces base-forward static instability. However, it is clearly apparent that symmetry in the pitching-moment curve does not exist since more area is enclosed by the negative portion of the curve than by the positive portion. This asymmetry in the pitching moment could lead to a potentially dangerous dynamic behavior during a reentry in which the vehicle is initially tumbling. A nonvanishing moment integral over a tumble cycle produces an energy transfer that could either enhance or decay the tumble rate, depending upon the direction of tumble. Since this possibility is avoided if the moment curve is symmetric, as would be the case for a symmetric model, the asymmetric fences were not further considered.

Symmetric but unvented fences (the complete series not shown) mounted directly on the model base also proved to be unsatisfactory. Such fences form a cavity which when oriented into the flow cause a nearly stagnant region. The details of the cavity are apparently unimportant in such a flow region and consequently the configuration reacts much like a flat disc facing broadside to the flow. Calculations showed that if the flared portion of these fences had not been obscured by the lack of flow within the cavity, they would have provided the necessary destabilizing moments. In order to improve the flow over the inner portion of these fences a new concept evolved in which the fences were mounted on pylons, thus providing a relief area through which some of the mass flow captured by the fence could escape. To evaluate this hypothesis, preliminary tests of two such vented fences on free-flying models were made in the 42-inch shock tunnel. The results showed the concept to be successful and a more detailed investigation was then undertaken with sting-mounted models in the 3.5-foot hypersonic wind tunnel. Results from those tests and from preliminary tests are presented in figures 10 and 11. It is apparent that the addition of either a conical or cylindroconical vented fence causes the nose-forward static stability to increase and the base-forward static stability to decrease.

While results obtained for the free-flying and for the sting-mounted models are generally similar, an important difference in the base-forward moment coefficients is apparent in the results shown in figures 10(a) and 11(a). In the tests of the sting-mounted models neither fence completely eliminated the angle-of-attack range over which the configurations would seek the base-forward attitude in flight. This is in contrast to the results for the free-flight tests which show the model with the cylindroconical fence to have neutral base-forward stability and the model with the conical fence to be unstable at an angle of attack of 180°. Several factors are believed to contribute to the differences observed between the two sets of test results. The effectiveness of the fence is strongly dependent upon the position of the shock wave relative to the fence. The closer the shock wave is to being attached to the trailing edge of the fence the more effective the fence is in producing an overturning moment. The shock wave standoff distances were less in the tests of the free-flight models for two reasons: the fences had sharper trailing edges and the more pronounced real-gas effects (higher enthalpy and Mach number) caused the density ratios across the shock waves to be higher (see ref. 8).

The effect of fence trailing-edge thickness on the effectiveness of producing overturning moments was investigated further in a series of tests made with sting-mounted models having fences with sharp trailing edges. Results of these tests are presented in figure 12. For comparison purposes, data are shown that were previously presented for the blunt-edge fences and for an unvented fence. The data show that all of the vented fences having sharp trailing edges were effective in eliminating the base-forward stability.

The largest amount of base-forward instability was produced by the extended cylindroconical fence. This results from the longer moment arm for the pressures acting on the fence and also from the greater variation in shock strength around the periphery of the fence. It should be noted that the latter would not occur without the abundant flow relief area provided by this particular fence.

The models with sharp trailing edged fences were not tested over the entire angle-of-attack range. Their aerodynamic characteristics, however, should not be sensitive to the fence trailing edge at the lower angles of attack. Therefore, curves of pitching-moment coefficients for the models with sharp-edged conical and cylindroconical fences over the entire angle-of-attack range can be obtained by pairing together results obtained with blunt-edged fences at lower angles of attack and results obtained with sharp-edged fences at higher angles of attack. The composite curves are shown in figure 13 where they are compared to the no-fence results. Composite results for the normal- and axial-force coefficients can be obtained in a similar manner.

The pressure measurements presented in figure 14 show the influence of various fences on the model base when it is oriented into the flow. In nearly all cases the pressure distributions show that the pitching moment due to the flat base of the body is unfavorable; that is, it returns the model to the base-forward attitude. This implies that the destabilizing effects of the fences result from aerodynamic loads on the fences themselves and not from the alterations of the pressures on the flat base due to the fences. The only significant departure from the no-fence case at zero angle of attack occurs near the periphery where harmonic-like variations are created by the flow being channeled through the relief holes. The high-pressure zone resulting from the extended fence at angle of attack (fig. 14(e)) apparently stems from a substantially weakened shock on the fence over this locality, thus providing further evidence as to why greater instability is observed with this fence.

Shadowgraphs obtained for the sting-mounted models tested at a Mach number of 7.4 with and without fences having sharp trailing edges are presented in figure 15. For attitudes near 180° the shock waves about all models with fences appear to have a larger radius of curvature and a smaller standoff distance than about the model with no fence. The shock wave attaches to the windward edge of the fence at an angle of attack between 160° and 170°. When attachment occurs, the local angle of attack of the flared surface near the attachment point is finite for the cylindroconical fence and nearly zero for the conical fence. This probably accounts for the fact that the pitching moment for the model with the cylindroconical fence is abruptly nonlinear in this angle-of-attack range while that for the conical fence model varies smoothly (see fig. 13).

Transonic Aerodynamic Characteristics

Static aerodynamic characteristics of the model with the cylindroconical fence are presented in figure 16. These data show that the quasi-linear static stability (fig. 16(a)) generally increased with increasing Mach number and increasing angle of attack. The marked increase in stability as the average resultant angle of attack is increased from values of the order of 6° to 35° may be attributed in large measure to the aerodynamic fence on which shock waves develop as it becomes "visible" to the flow. The drag coefficients (fig. 16(b)) increased with increasing Mach number, and the slope of the lift-coefficient curve (fig. 16(c)) was negative for all test conditions. The latter characteristics are representative of those for high-drag bodies of revolution.

Shadowgraphs illustrating the shock wave development as the angle of attack increases are presented in figure 17. For Mach numbers near 1.2 the fence is shown to be within the model wake for angles of attack up to about 15°. With increased angle of attack a portion of the fence becomes exposed to the flow, causing an attached shock wave, which detaches, moves forward, and finally interacts with an expansion wave as the angle of attack exceeds 30°. When the fence is completely buried in the wake, it does not contribute significantly to the static stability. However, once this fence is exposed to the stream the pressure on the windward side exceeds that on the leeward side, thus producing a stabilizing moment. Because of the more rapid wake closure at higher Mach numbers, the fence will become exposed at smaller angles of attack and the aerodynamic coefficients may be expected to be more nearly linear.

The dynamic aerodynamic results obtained for this configuration are shown figure 18. These data show that the models were dynamically unstable over the ranges of conditions investigated. This instability appears to become less severe with increasing pitch amplitude; however, the existence of a limit cycle was not established experimentally. Data were not obtained for amplitudes larger than 38°.

Although the blockage factor relative to the test vessel was 0.03 percent, intermittent passage of the model through blast shield openings (which provide instrument protection at each data station) gave blockage factors ranging from 0.28 to 1.03 percent. Some scatter in the data (particularly the more sensitive dynamic stability parameter) may be attributed to the asymmetrical effects of blockage (appearing as unnatural local velocity gradients compounded by reflected shock waves); however, the magnitude of this influence was not investigated.

Trajectory Analysis

It has been shown that the base-forward static aerodynamic stability of the 60° half-angle blunted cone can be eliminated by the addition of an aerodynamic fence-type afterbody. It remains to be determined if the degree of base-forward instability provided by such a fence is adequate to turn a vehicle around before it encounters severe aerodynamic heating after entering the atmosphere base forward. A six degree-of-freedom trajectory computer program was used to study this situation.

The vehicle characteristics (mass properties and geometry) resulting from the preliminary design study of the isotope reentry vehicle of reference 1 were chosen for this analysis. These are:

Maximum diameter:	2.16 m
Mass center:	0.61R from nose
Mass:	834.7 kg
Spin-axis moment of inertia:	273.8 kg-m^2

Pitch-axis moment of inertia Yaw-axis moment of inertia	149.5 kg-m^2

The experimentally obtained static hypersonic aerodynamic coefficients for the configuration having the conical fence with sharp trailing edge were assumed to apply at all Mach numbers above 2. The unknown hypersonic damping-in-pitch derivative was originally taken as zero. Small deviations of this quantity from zero proved to have a negligible effect on the resulting trajectory during the period of rising dynamic pressure. However, the oscillatory motion became quite sensitive to the value of this derivative once the dynamic pressure began to decrease. Hence, for the calculations, a conservative value of zero was used for the portions of the trajectories up to peak dynamic pressure while a more realistic value of -0.1 (see ref. 9) was assumed to apply beyond peak dynamic pressure down to a Mach number of 2. For Mach numbers below 2 aerodynamic results from the transonic tests were used. The static coefficients were obtained from the data fairings shown in figure 16. The drag coefficient was well represented by a function of Mach number alone while the lift and moment coefficients were functions of Mach number and linear functions of angle of attack. Somewhat synthetic estimates of the damping-in-pitch derivative indicated by the faired curves in figure 18(b) were used. Values required for pitch amplitudes exceeding 15° were obtained by extrapolation.

In general, an uncontrolled entry involves an arbitrary initial angular rate and a random initial angle of attack as the vehicle reaches the sensible atmosphere. For severe, but limited, initial tumble rates, the results of reference 2 show that an upper bound for the amplitude of subsequent angle-of-attack histories is given fairly well by assuming base-forward entry with zero initial tumble rate. However, entry at an angle of attack near 180° will yield a predicted trajectory in which the vehicle would remain in this unstable but trimmed attitude over most of its descent. It is argued in reference 2 that correct physical modeling accounting for angle-of-attack perturbations due to atmospheric irregularities would no doubt reduce the probability of a sustained base-forward flight and that a realistic compromise is to consider initial angles of attack displaced a few degrees from an unstable trim point. This is further justified by the effective angle of attack which inevitably results from flight path curvature during the course of vehicle descent. Therefore, instead of investigating a rather large family of reentry conditions, the trajectories were initiated with a tumble rate of zero and an angle of attack of 175°.

Two calculated trajectories of the vehicle entering the Earth's atmosphere are presented in figure 19. For an initial roll rate of zero the results show that the vehicle turns around 90° so that the unprotected base will be aft before the stagnation-point heating increases to 20 percent of peak value. It is further shown that an initial roll rate of 1 rad/s clearly adds an undesirable measure of gyroscopic stability; however, the vehicle does turn around 90°, so that the base is aft by the time the stagnation-point heating rate reaches 50 percent of maximum value. Peak heating rate for both cases occurred after a 60-s descent to an altitude of about 46 km (150,000 ft).

For the same initial conditions as above and with a roll rate of 1 rad/s, the resulting motion down to a Mach number of 0.8 is presented in figure 20. The envelope of angle of attack is seen to converge until the vehicle reaches 11° at a Mach number of 2.0 whereupon the vehicle becomes

dynamically unstable. The subsequent growth and decay in amplitude follow the same trend as established by the damping-in-pitch derivatives given in figure 18(b). Thus, for these aerodynamic characteristics, the maximum amplitude predicted for the critical transonic flight regime is 57°.

Clearly each trajectory analysis is dependent on the liberties taken in building a continuous and complete aerodynamic description founded on limited experimental tests. The predicted trajectory in figure 20 should, therefore, not be used to infer broad trends without carefully reviewing the aerodynamic characteristics imposed. For example, each of the following motions was calculated for a vehicle without roll. Letting the damping-in-pitch derivative be zero produced oscillations which diverged to 110° after the vehicle reached a Mach number of 2.0, whereas a value of +0.04 resulted in a tumbling motion before this point was reached. Up to the point of peak dynamic pressure, however, both cases were found to differ by only a few degrees. Choosing a more realistic value of -0.1 for this derivative resulted in oscillations that converged to 6° at a Mach number of 2.0. Below this Mach number transonic test data were assumed to apply and the oscillations then diverged to the point of tumbling. This unbounded divergence was attributed to the planar motion arising from zero roll which permitted large positive damping-in-pitch derivatives to be experienced as the vehicle oscillated through zero angle of attack. It is clear, therefore, from figure 20 that the nonplanar motion produced by roll successfully limited the growth in amplitude during the critical transonic flight regime. Although the effect is beneficial during this subsequent phase of nose-forward oscillations, there will be an upper limit on the magnitude of roll permitted such that a nontumbling vehicle during the initial reentry phase will not become spin-stabilized in a base-forward attitude.

CONCLUDING REMARKS

It has been shown experimentally that it is possible to eliminate the base-forward stable trim point by adding a fence-type afterbody; however, only symmetric fences are judged suitable from the standpoint of an uncontrolled reentry. Hypersonic tests indicate that the fence should be vented and trailing-edge sharpened to yield the greatest base-forward instability. Transonic tests indicate that nose-forward dynamic instability may exist for pitching amplitudes as high as 40°. A trajectory analysis showed that the vehicle would be oriented in nose-forward flight well before peak heating, even under severe reentry conditions. The variation in angle-of-attack envelope, however, was not monotonic over the entire trajectory and large amplitudes recurred during the transonic flight regime. It was found that these amplitudes could be bounded by having the vehicle roll as it entered the atmosphere, thus causing the motion to be nonplanar, and thereby avoiding small amplitudes where the damping-in-pitch would be destabilizing.

Ames Research Center
and
U.S Army Air Mobility R&D Laboratory
National Aeronautics and Space Administration
Moffett Field, Calif., 94035, January 21, 1971

REFERENCES

1. Ryan, R. L.; et al.: Isotope Reentry Vehicle Design Study, Preliminary Design: Phase 2. Final Report (NAS 3-10938) NASA CR-72555, 1969.

2. Peterson, Victor L.: Motions of a Short 10° Blunted Cone Entering a Martian Atmosphere at Arbitrary Angles of Attack and Arbitrary Pitching Rates. NASA TN D-1326, 1962.

3. Sammonds, Robert I.: Transonic Static- and Dynamic-Stability Characteristics of two Large-Angle Spherically Blunted High-Drag Cones. AIAA Paper 70-564, 1970.

4. Loubsky, William J.; Hiers, Robert S.; Steward, David A.: Performance of a Combustion Driven Shock Tunnel with Application to the Tailored-Interface Operating Conditions. Presented at the 3rd Conference on Performance of High Temperature Systems, Pasadena, Ca., Dec. 7-9, 1964.

5. Hiers, Robert S., Jr.; and Reller, John O., Jr.: Analysis of Nonequilibrium Air Streams in the Ames 1-Foot Shock Tunnel. NASA TN D-4985, 1969.

6. Ames Research Center Staff: Research Facilities Summary. Vol. I - Guns and Ranges. NASA TM X-59,258, 1965.

7. Malcolm, Gerald N.; and Chapman, Gary T.: A Computer Program for Systematically Analyzing Free-Flight Data to Determine the Aerodynamics of Axisymmetric Bodies. NASA TN D-4766, 1968.

8. Katzen, E. D.; and Kaattari, G. E.: Inviscid Hypersonic Flow Around Blunt Bodies. AIAA J., vol. 3, no. 7, July 1965, pp. 1230-1237.

9. Marko, W.: Dynamic Stability of High-Drag Planetary Entry Vehicles at Transonic Speeds. AIAA Paper 69-105, 1969.

TABLE 1.- FENCE DIMENSIONS

Facility / Geometry	42-Inch shock tunnel				3.5-Foot hypersonic wind tunnel				Pressurized ballistic range			
	Dia., cm	Length	Trailing edge thickness	Flare angle, deg	Dia., cm	Length	Trailing edge thickness	Flare angle, deg	Dia., cm	Length	Trailing edge thickness	Flare angle, deg
Asymmetric fence	10.2	0.2R	0.031R	0	—	—	—	—	—	—	—	—
	9.0	0.2R	0.31R	-16.7	—	—	—	—	—	—	—	—
	9.0	0.2R	0.31R	-30.0	—	—	—	—	—	—	—	—
Cylindro-conical (unvented)	—	—	—	—	20.3	0.5R	0.031R	36.6	—	—	—	—
Cylindro-conical (vented)	12.7	0.5R	0.025R	36.6	20.3	0.5R	0.031R	36.6	5.08	0.5R	0.053R	36.6
	—	—	—	—	20.3	0.5R	0.0005R	43.0	—	—	—	—
Conical (vented)	12.7	0.5R	0.025R	14.0	20.3	0.5R	0.047R	14.0	—	—	—	—
	—	—	—	—	20.3	0.5R	0.0005R	24.0	—	—	—	—
Extended (vented)	—	—	—	—	20.3	0.7R	0.031R	36.6	—	—	—	—
	—	—	—	—	20.3	0.7R	0.0005R	43.0	—	—	—	—

TABLE 2.- MODEL AND TRANSONIC FLIGHT DATA WITH CYLINDROCONICAL FENCE

Test	Mass, g	d, cm	x_{cg}, cm	I, g-cm^2	Stations	M	Re$\times 10^{-6}$	α_m, deg	α_{rms}, deg	C_D	$-C_{L_\alpha}$	$-C_{m_{\alpha_l}}$	ξ	$C_{m_q} + C_{m_{\dot{\alpha}}}$
1382 ○	267.3	5.084	1.426	508.6	2-12	1.05	1.217	6.18	3.97	1.295	1.005	0.146	14.171	0.873
					6-15	1.01	1.165	7.87	5.32	1.255	.892	.135	11.782	.709
					8-19	.96	1.113	8.87	6.05	1.155	.847	.126	4.441	.179
					10-21	.93	1.077	9.31	6.34	1.099	.814	.123	2.234	.024
					14-24	.89	1.027	9.58	6.56	1.042	.774	.125	.112	-.125
1383 □	265.8	5.084	1.431	507.5	3-12	1.15	1.302	5.49	3.76	1.327	.959	.154	19.132	1.244
					6-16	1.10	1.246	6.56	4.82	1.321	.956	.148	11.055	.648
					8-19	1.05	1.192	7.68	5.84	1.309	1.029	.149	8.129	.428
					11-21	1.01	1.137	8.78	6.74	1.266	.945	.137	8.542	.468
					14-24	.96	1.089	9.33	7.51	1.140	.914	.134	5.012	.219
1384 ◇	266.7	5.081	1.434	510.5	2-12	1.25	1.441	4.37	2.92	1.343	1.026	.153	12.183	.727
					6-15	1.20	1.377	5.27	3.46	1.334	1.110	.147	12.610	.753
					8-18	1.15	1.320	5.79	3.86	1.317	1.137	.147	6.984	.336
					10-20	1.10	1.271	6.24	4.36	1.310	1.127	.151	3.959	.113
					14-23	1.04	1.200	6.58	4.51	1.290	1.057	.149	2.719	.028
1385 △	268.1	5.081	1.432	515.7	2-11	1.35	1.559	3.28	2.13	1.349	.972	.170	15.445	.977
					5-15	1.29	1.490	4.13	2.90	1.337	1.151	.158	11.603	.679
					8-17	1.24	1.433	4.86	3.34	1.324	1.085	.149	9.584	.534
					10-20	1.18	1.366	5.93	4.10	1.312	1.035	.146	10.612	.616
					13-22	1.13	1.311	6.79	4.63	1.300	1.013	.144	10.746	.628
					16-24	1.09	1.265	7.55	5.50	1.286	1.033	.141	7.717	.402
1386 ◺	268.0	5.083	1.435	514.1	3-13	.94	1.099	3.26	2.07	1.112	.740	.115	17.896	1.191
					6-17	.90	1.059	3.68	2.61	1.065	.666	.121	10.535	.653
					9-19	.87	1.019	4.10	2.85	1.043	.619	.125	3.841	.162
					12-22	.83	.976	4.69	3.40	1.017	.591	.125	5.244	.270
					15-24	.81	.947	5.06	3.45	.994	.561	.127	7.532	.444
1391 ⏢	267.4	5.085	1.434	511.9	3-11	2.00	2.362	11.36	8.13	1.419	1.094	.187	3.567	.078
					6-15	1.91	2.249	12.01	8.88	1.422	1.125	.185	3.656	.082
					8-17	1.84	2.171	12.55	8.82	1.418	1.104	.180	3.132	.045
					10-20	1.75	2.060	13.50	10.04	1.410	1.093	.177	3.782	.095
					13-22	1.67	1.969	14.27	10.60	1.407	1.130	.175	4.154	.120
					16-24	1.60	1.889	15.22	11.18	1.400	1.110	.172	4.144	.121
1392 ◹	266.2	5.081	1.424	509.5	3-13	1.04	1.205	6.93	5.15	1.295	1.105	.144	6.645	.315
					7-17	.99	1.147	8.03	6.12	1.214	.951	.133	9.536	.546
					9-19	.95	1.105	9.09	7.00	1.123	.915	.124	8.306	.465
					11-21	.92	1.070	9.38	7.68	1.066	.883	.121	3.052	.082
1393 ◇	267.1	5.083	1.423	511.0	1-12	1.21	1.420	6.07	4.16	1.341	1.129	.144	6.936	.331
					6-16	1.15	1.339	6.96	4.77	1.326	1.074	.141	5.049	.196
					8-19	1.10	1.280	7.52	5.12	1.318	1.105	.137	3.818	.103
					11-21	1.04	1.219	8.29	5.67	1.303	1.070	.140	4.877	.185
					14-24	1.00	1.163	9.33	6.49	1.220	.956	.137	6.520	.322
1395 ◊	266.3	5.081	1.424	511.3	1-11	1.19	1.377	32.26	23.00	1.276	.789	.231	1.670	-.029
					4-13	1.16	1.335	32.92	23.09	1.266	.776	.234	2.156	.009
					7-16	1.11	1.287	33.80	23.90	1.256	.756	.236	1.863	-.011
					9-18	1.07	1.241	34.51	24.10	1.249	.742	.238	1.157	-.062
					12-20	1.03	1.189	34.99	24.12	1.237	.727	.244	1.958	.0
					14-22	1.00	1.154	36.45	25.51	1.185	.680	.243	2.819	.071
					17-24	.97	1.116	37.79	26.53	1.101	.609	.236	3.079	.102

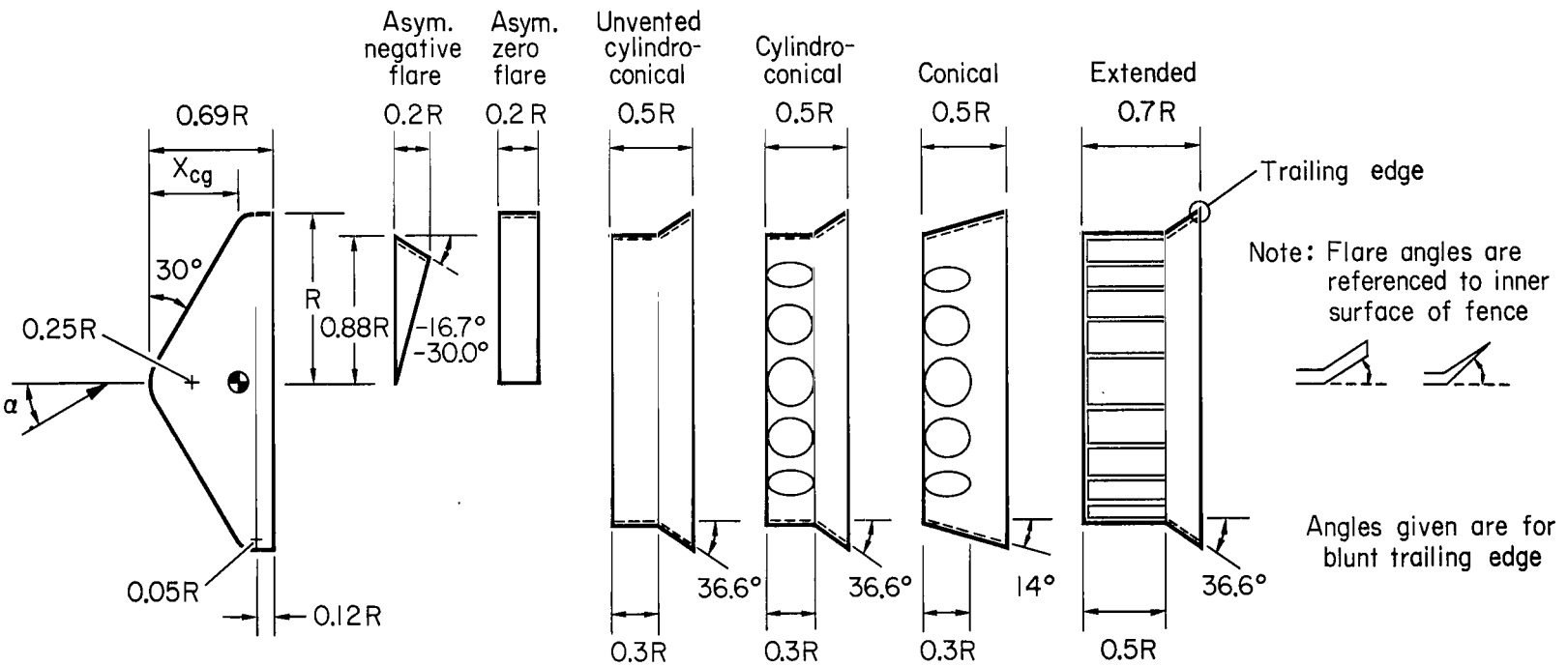

Figure 1.- Model geometry.

Figure 2.- Suspended model in Ames 42-Inch Shock Tunnel (combustion driven) prior to flight.

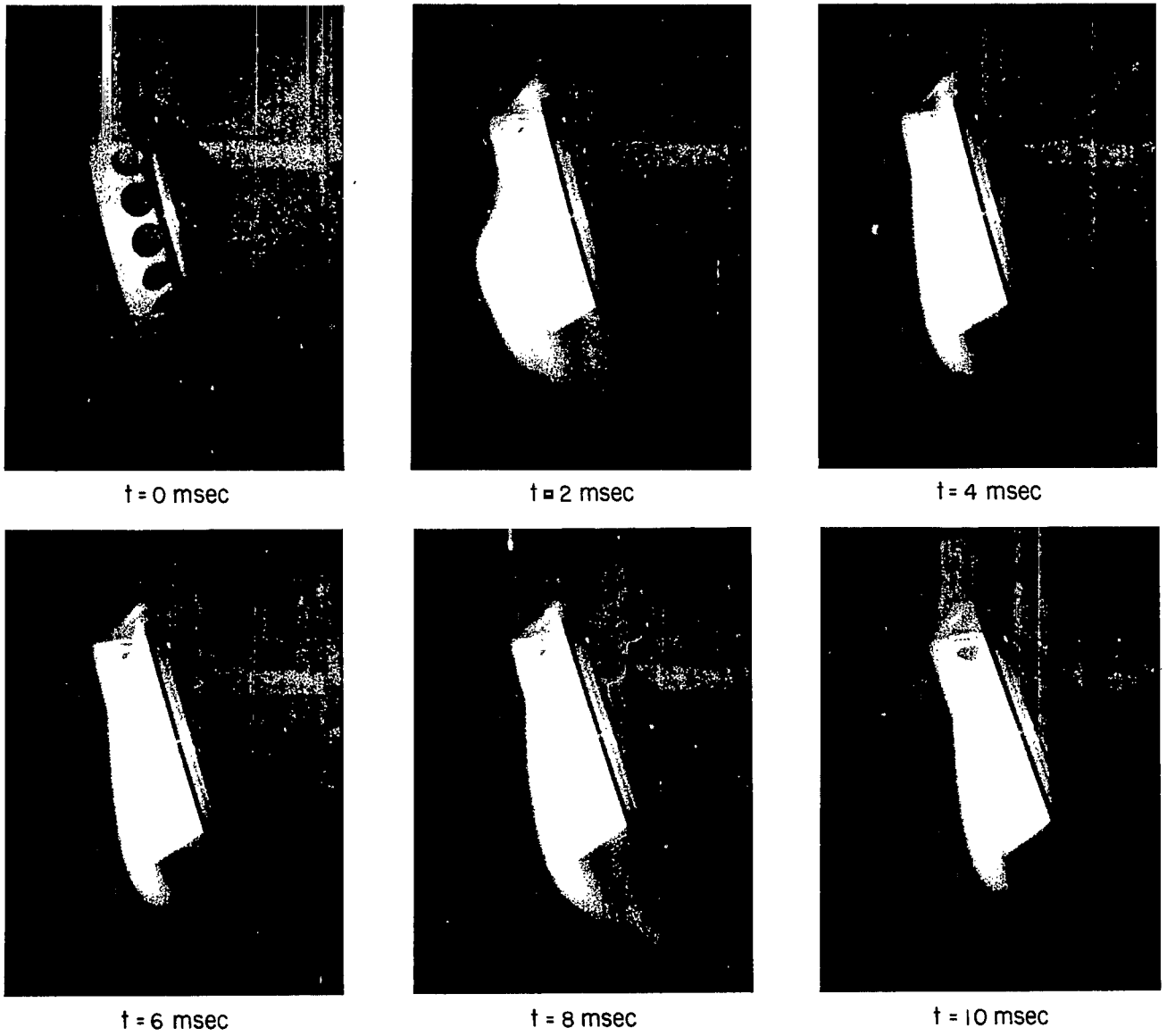

Figure 3.- Representative frames of motion pictures showing flow development and model flight at M = 12.5.

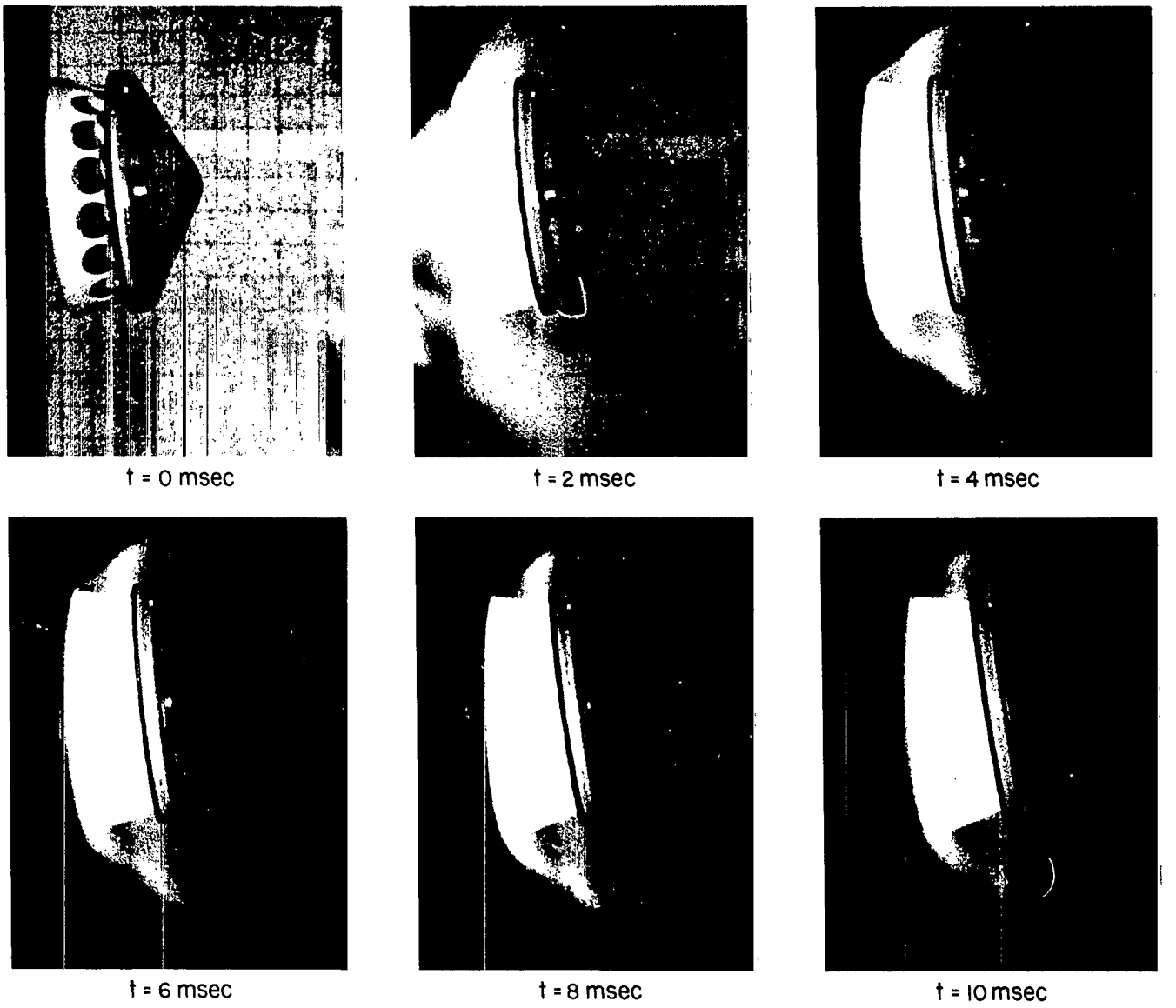

Figure 3.- Concluded.

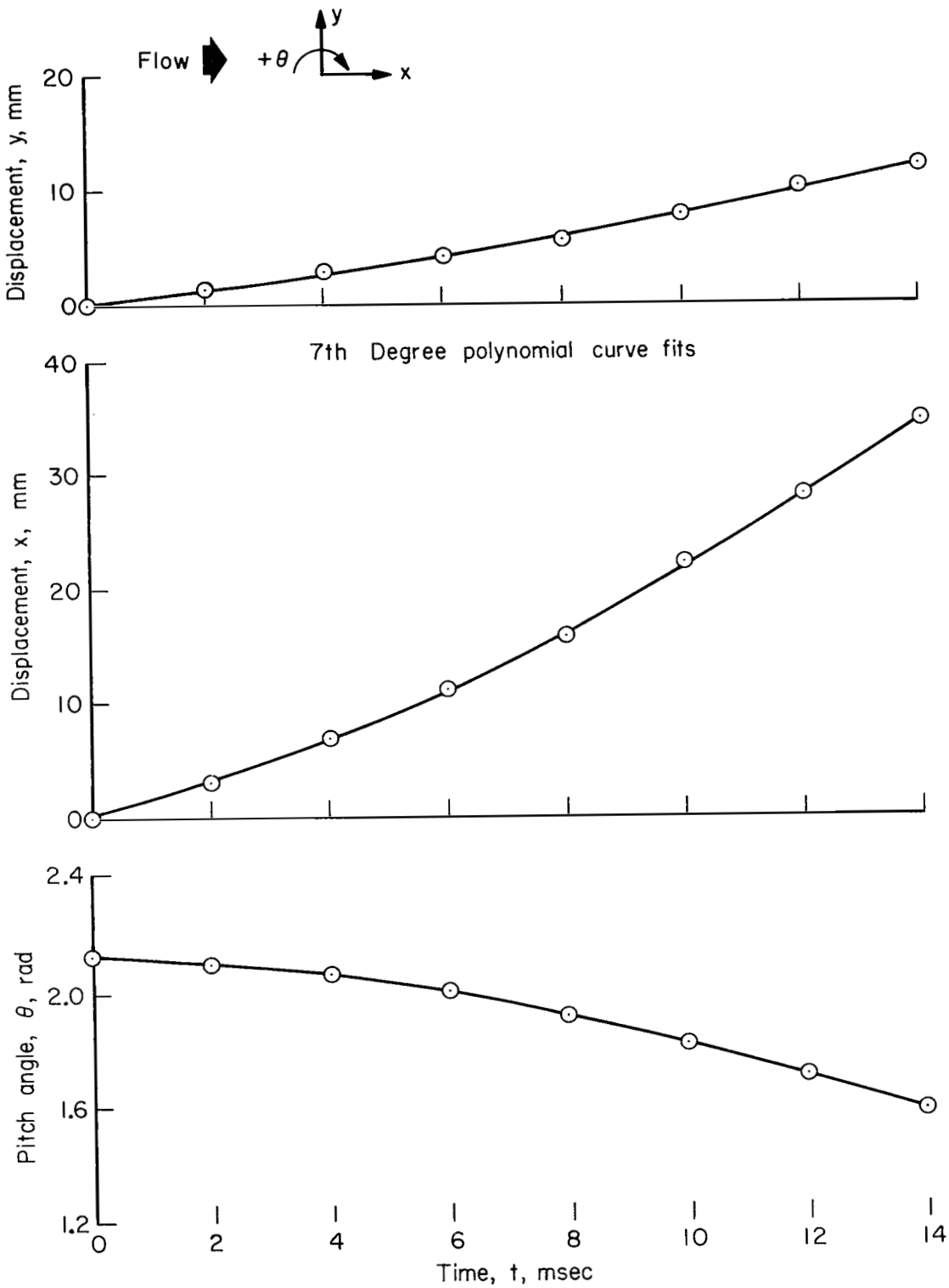

Figure 4.- Example of measured displacements from hypersonic free-flight tests.

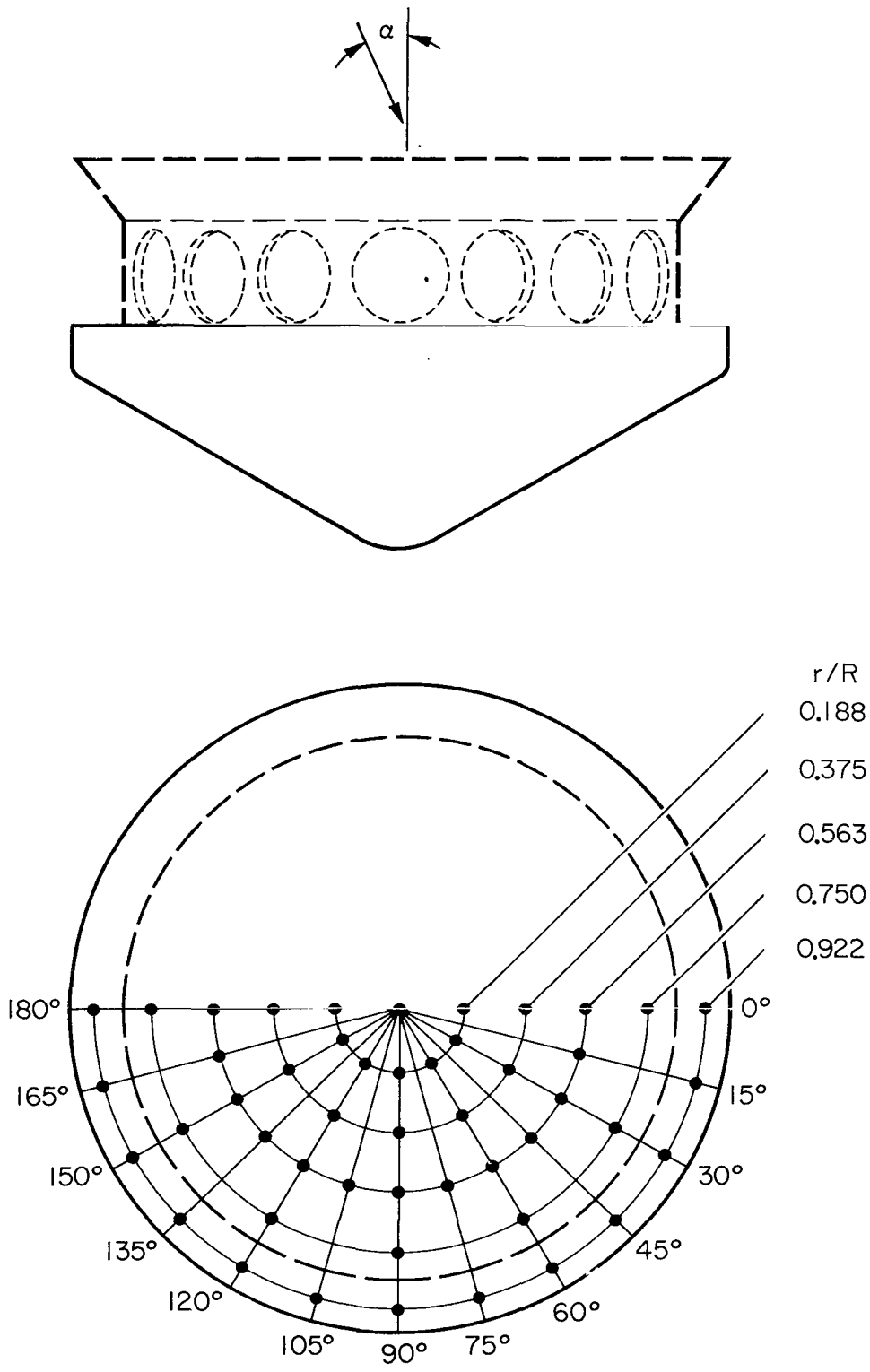

Figure 5.- Orifice coordinates.

Figure 6.- Sting-mounted model in Ames 3.5-Foot Hypersonic Wind Tunnel.

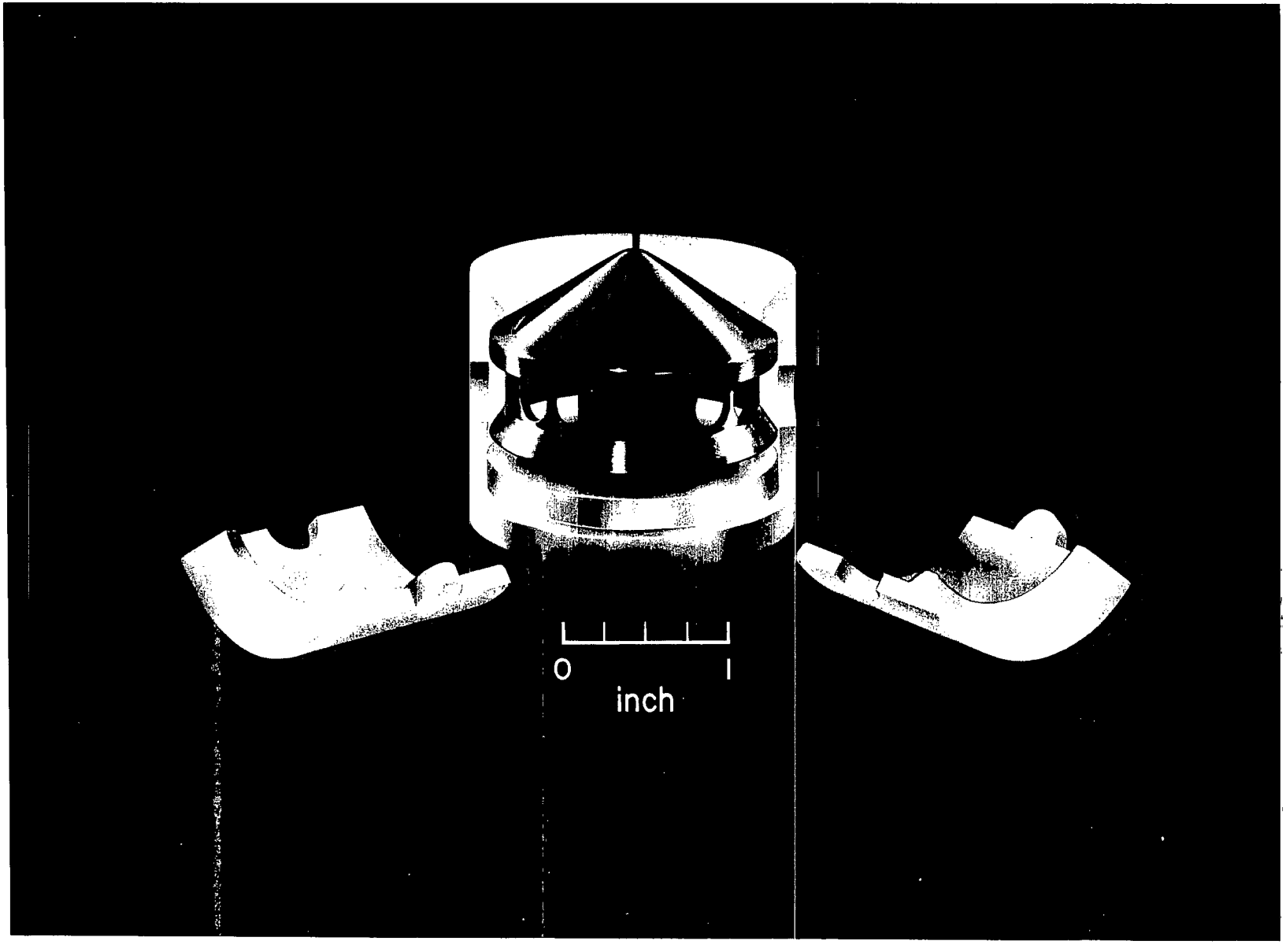

Figure 7.- Typical model and launch sabot used in transonic tests.

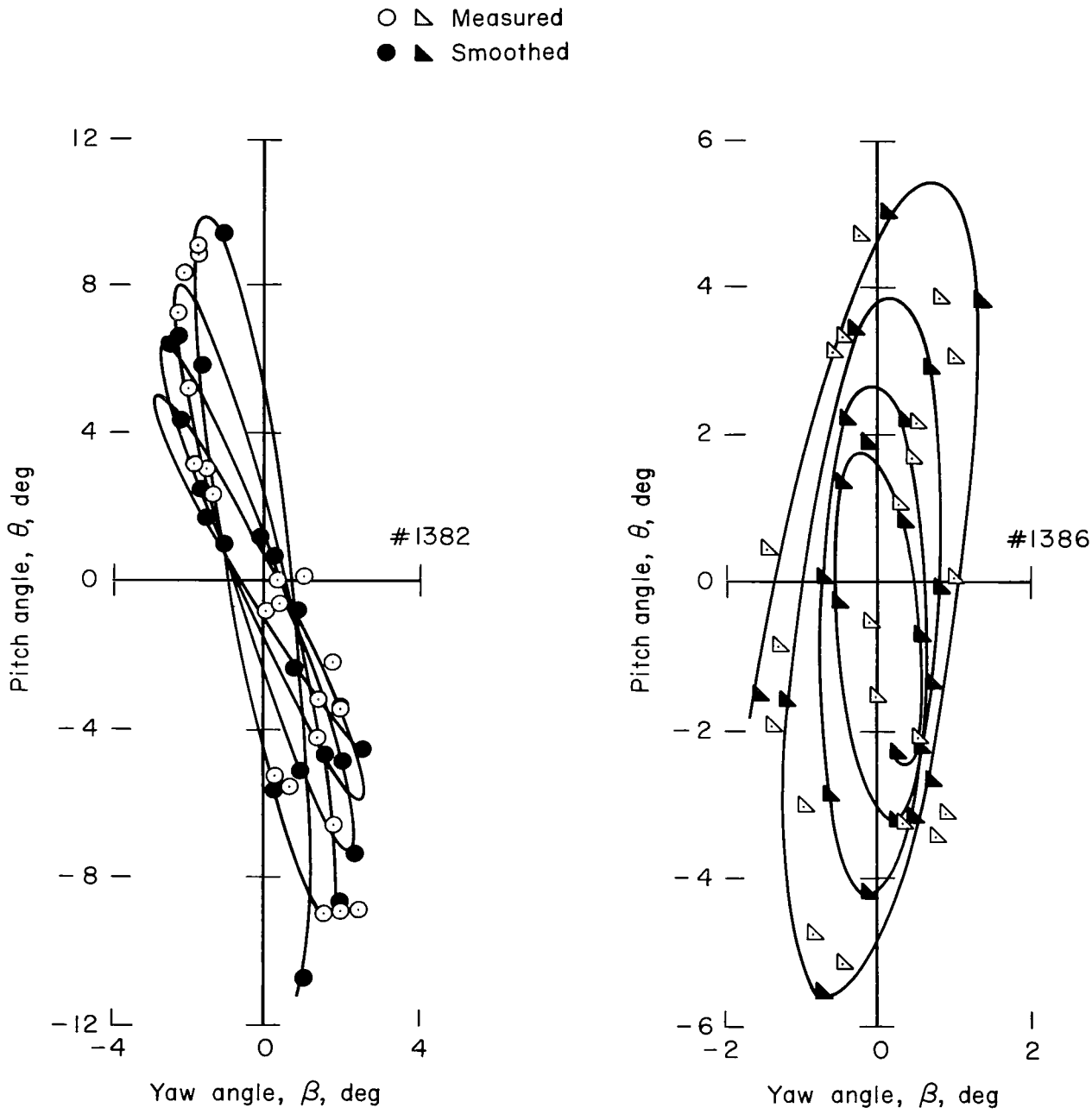

Figure 8.- Example of pitch and yaw displacements from transonic free-flight tests.

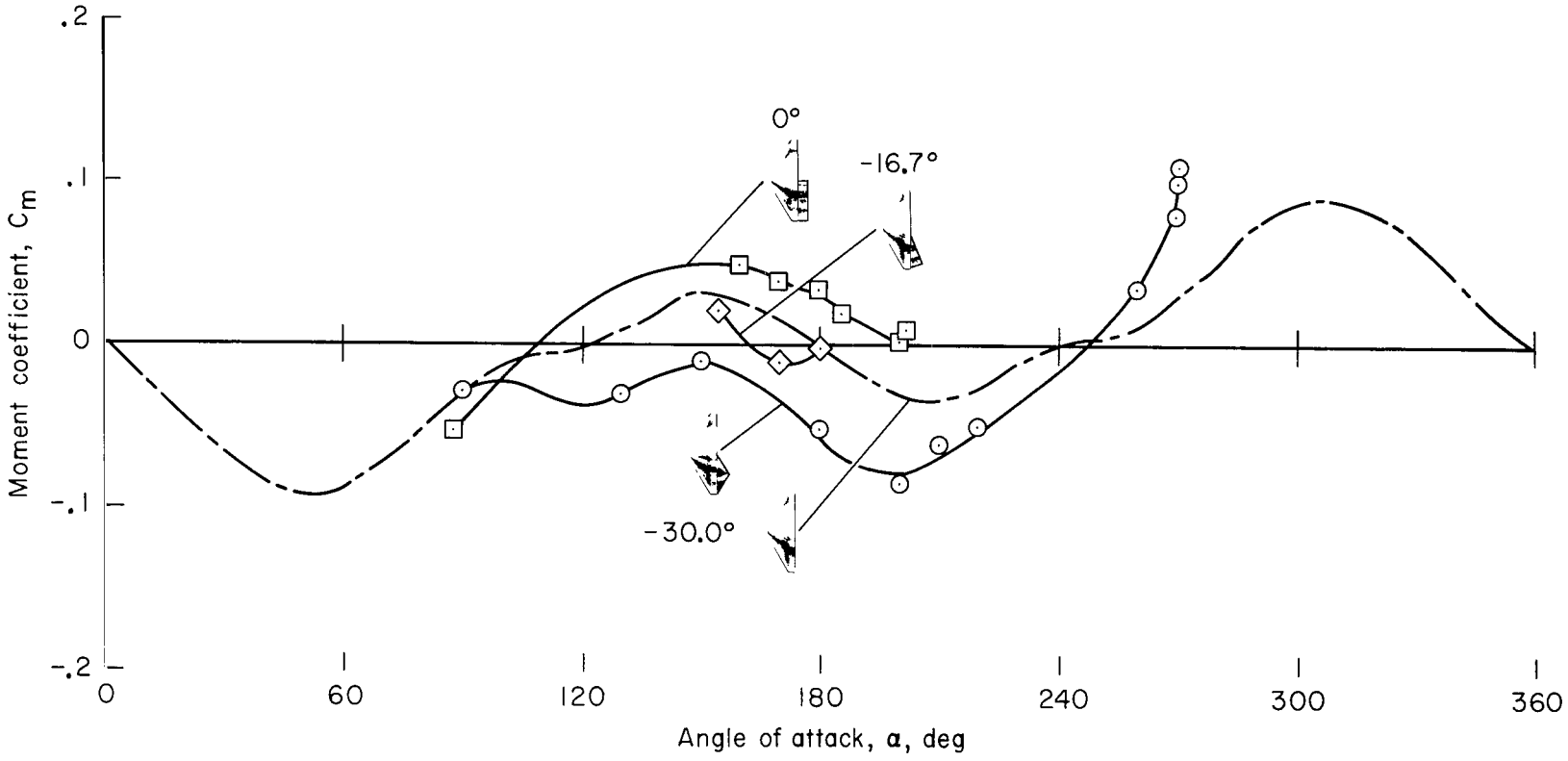

Figure 9.- Moment alterations resulting from asymmetric fences at M = 12.5.

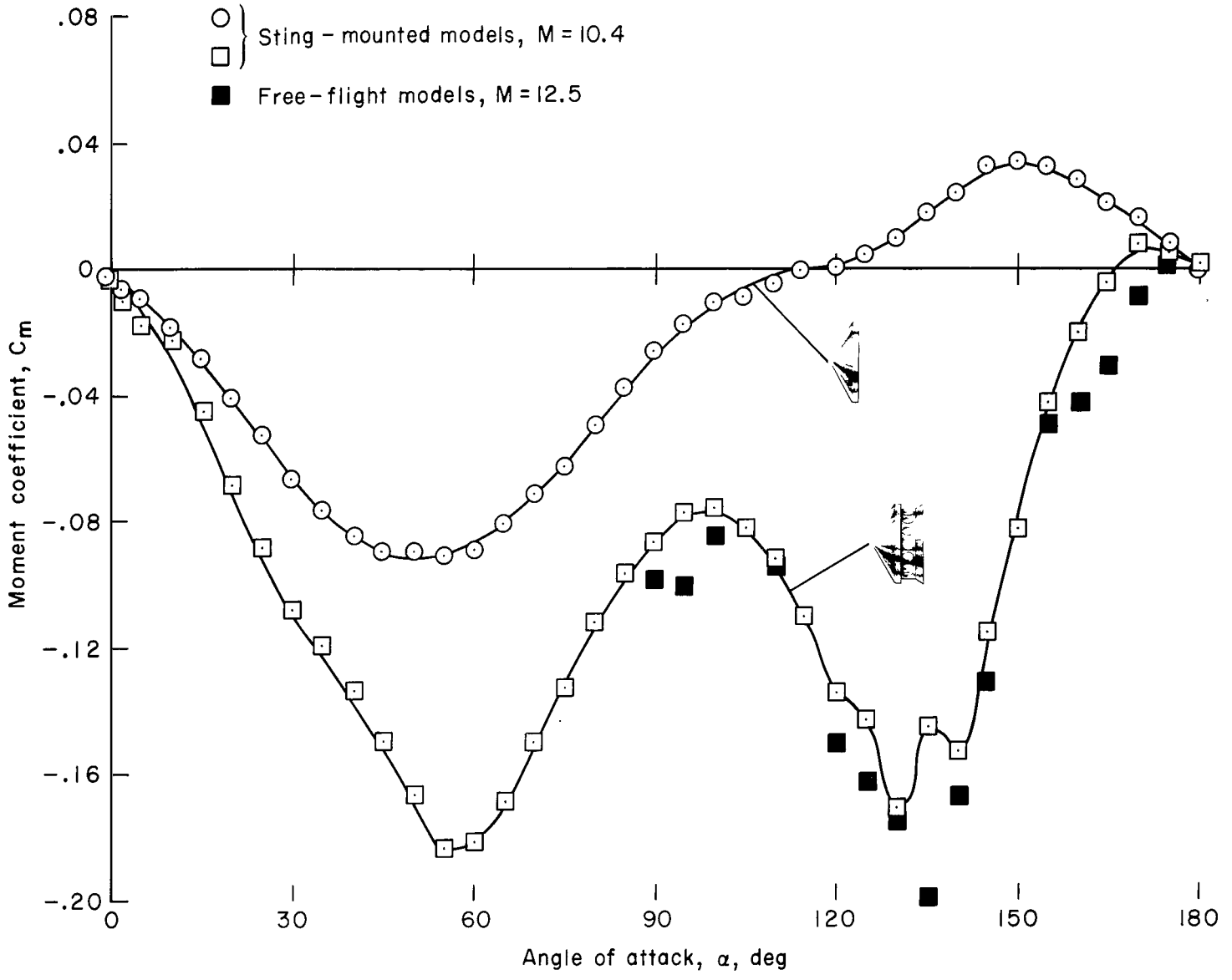

(a) Variation of pitching-moment coefficients with angle of attack.

Figure 10.- Pitching-moment, normal-force, and axial-force coefficients for models with and without cylindroconical fences.

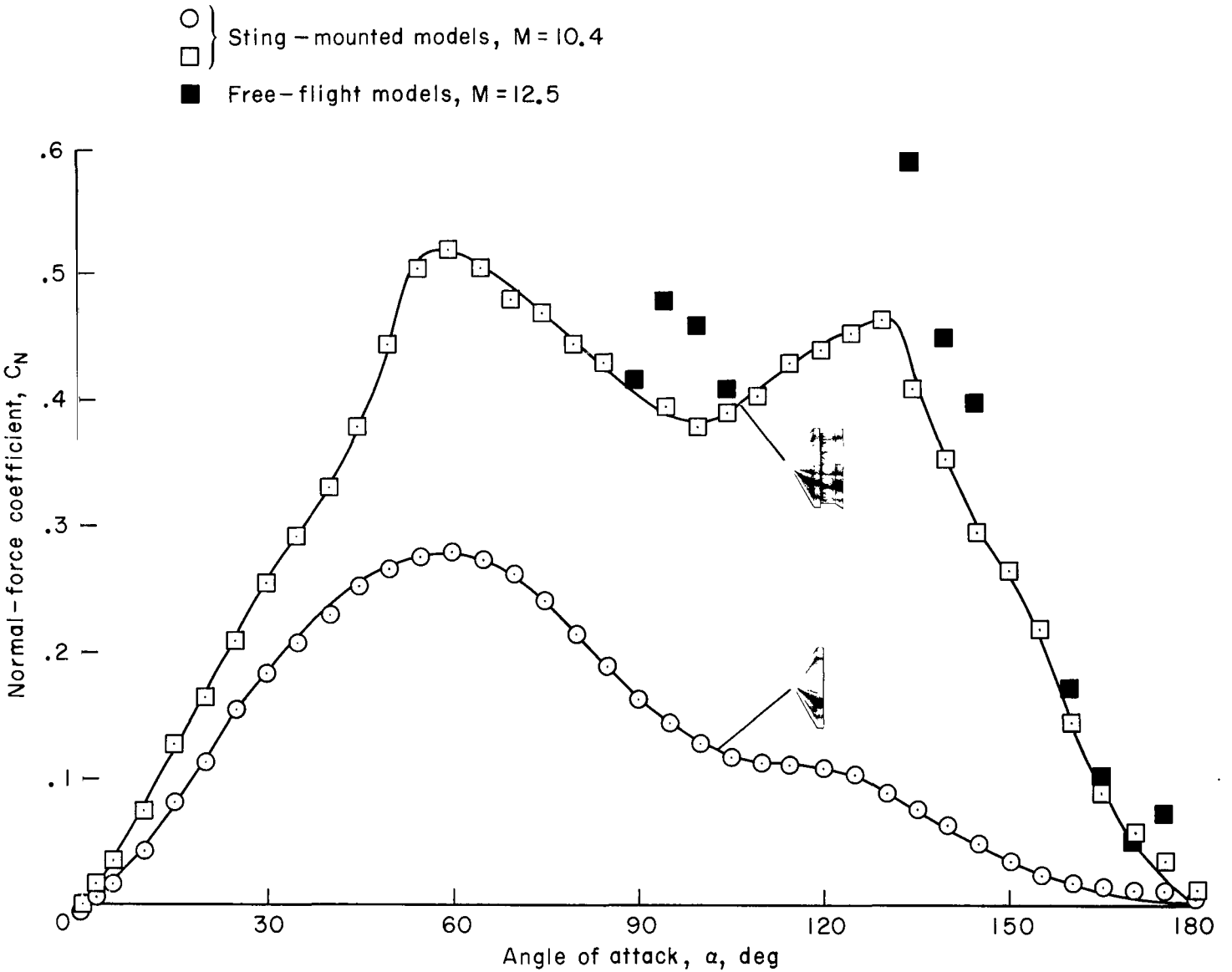

(b) Variation of normal-force coefficients with angle of attack.

Figure 10.- Continued.

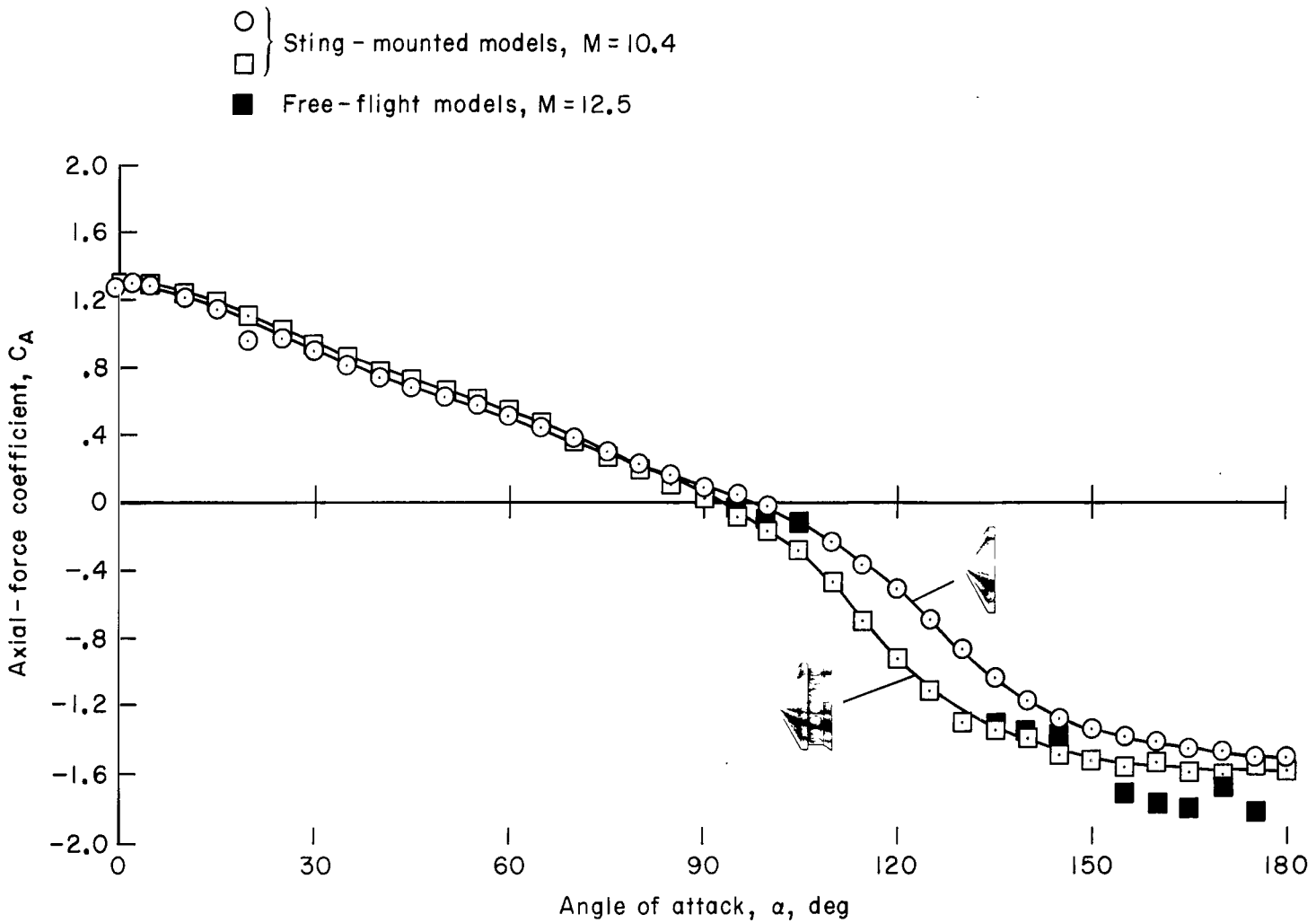

(c) Variation of axial-force coefficients with angle of attack.

Figure 10.- Concluded.

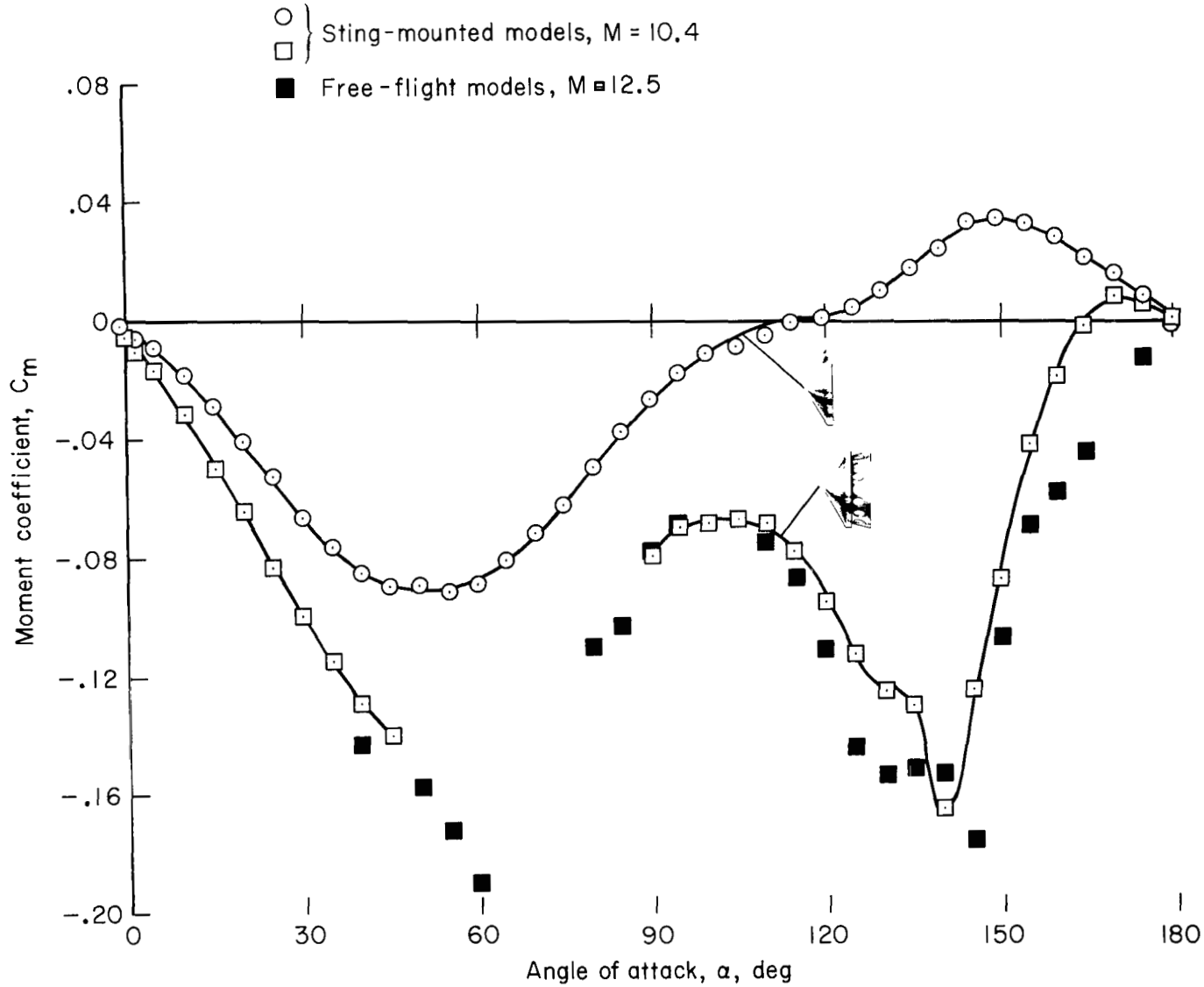

(a) Variation of pitching-moment coefficients with angle of attack.

Figure 11.- Pitching-moment, normal-force, and axial-force coefficients for models with and without conical fence.

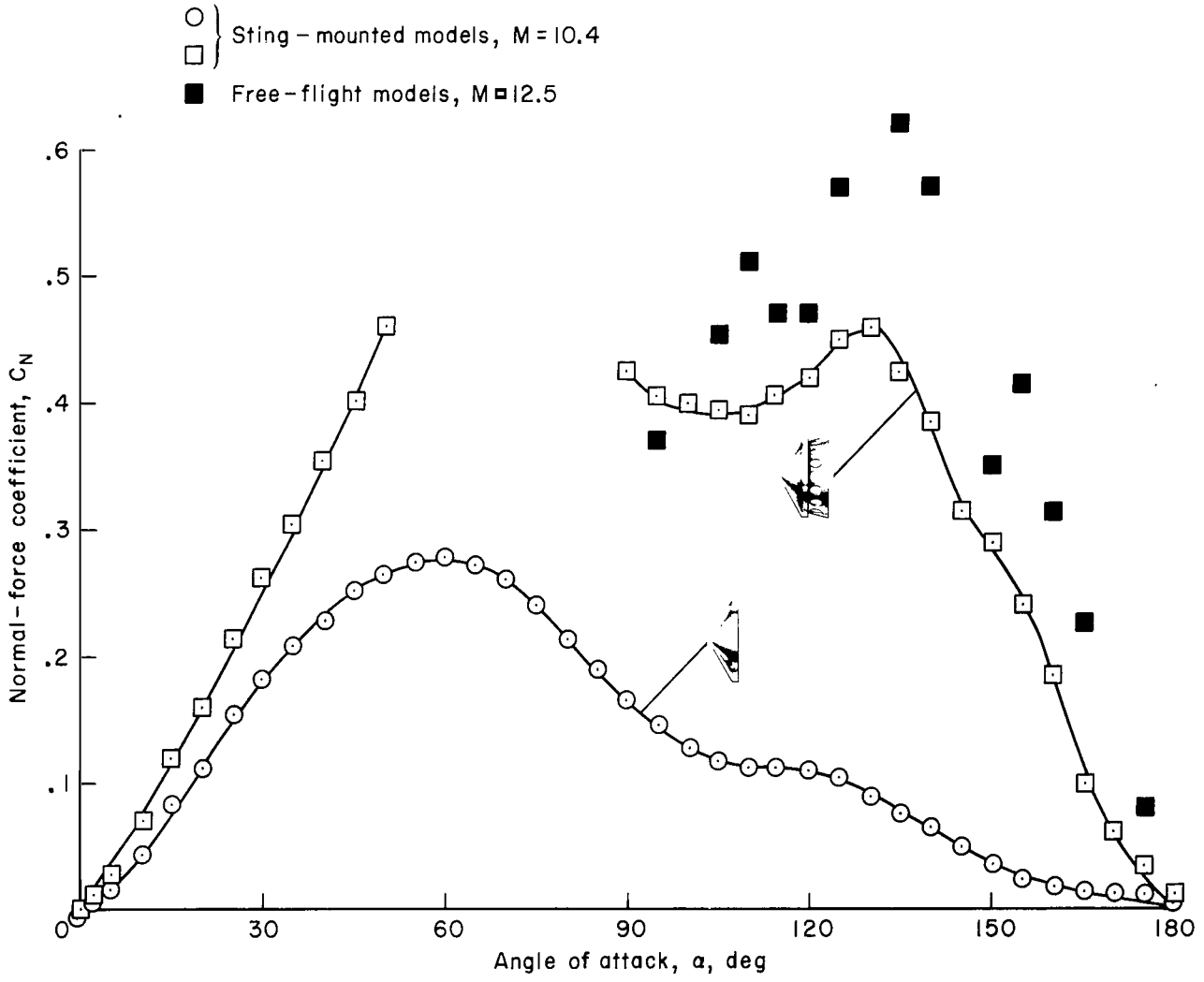

(b) Variation of normal-force coefficients with angle of attack.

Figure 11.- Continued.

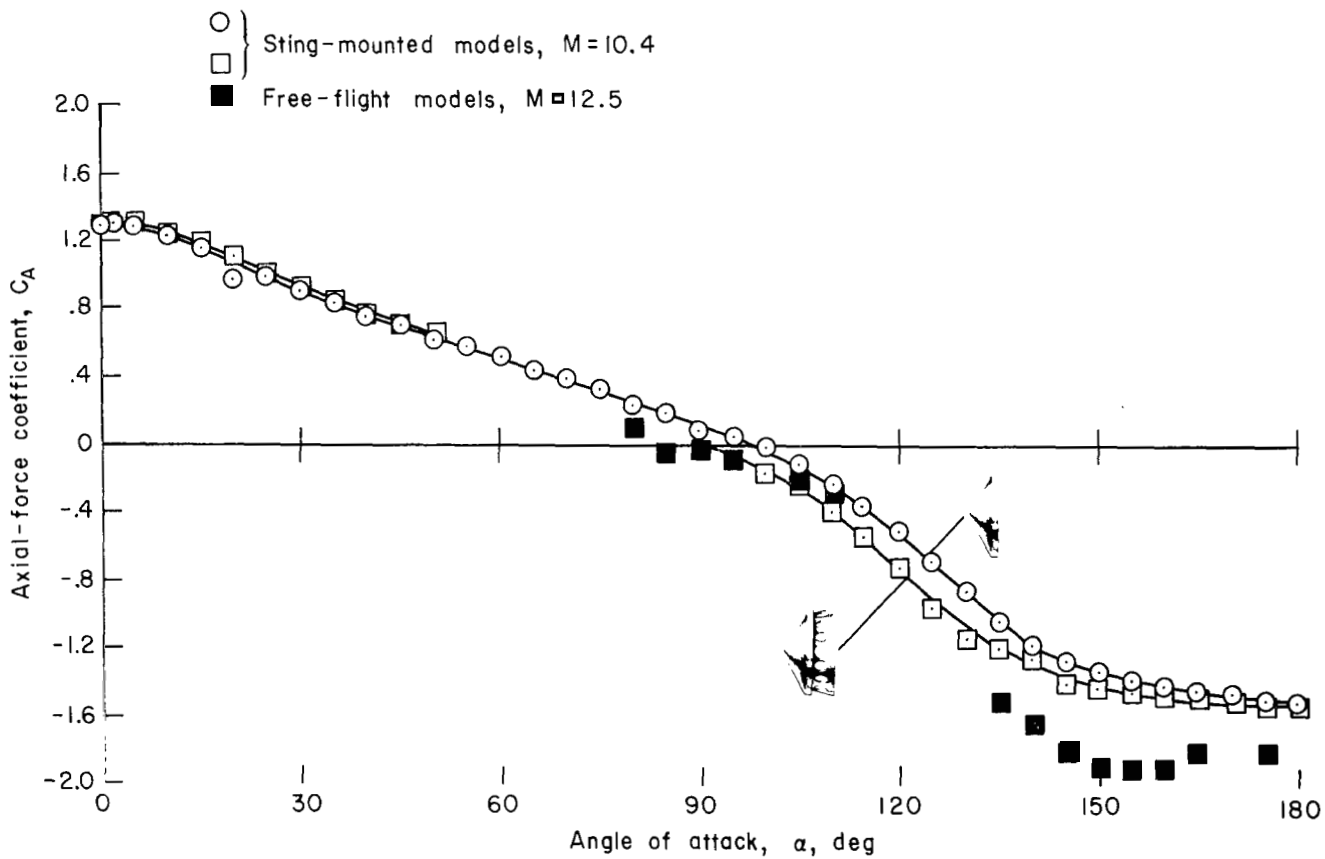

(c) Variation of axial-force coefficients with angle of attack.

Figure 11.- Concluded.

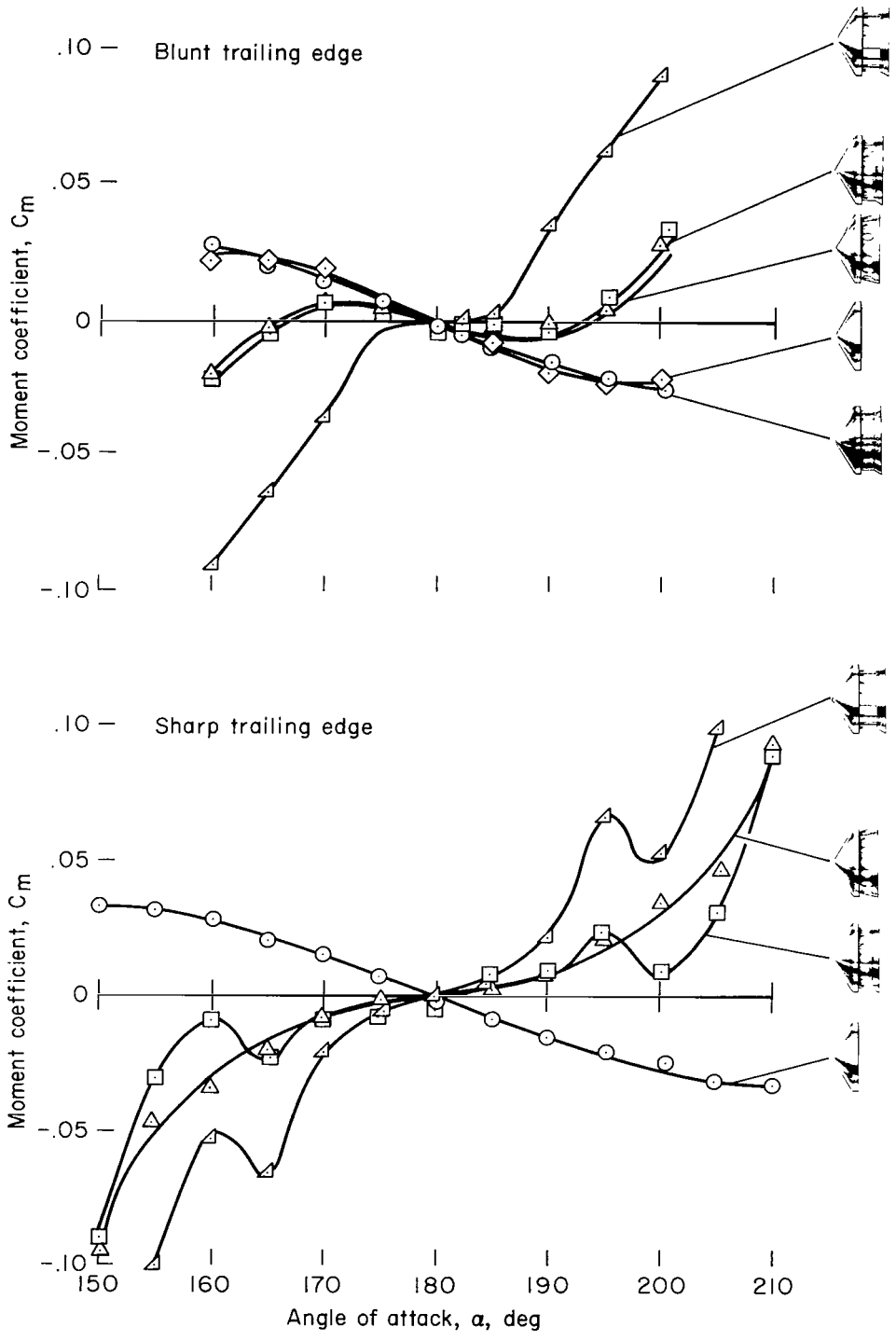

(a) Pitching-moment coefficients.

Figure 12.- Effects of fence trailing-edge bluntness on aerodynamic characteristics of sting-mounted models, M = 10.4.

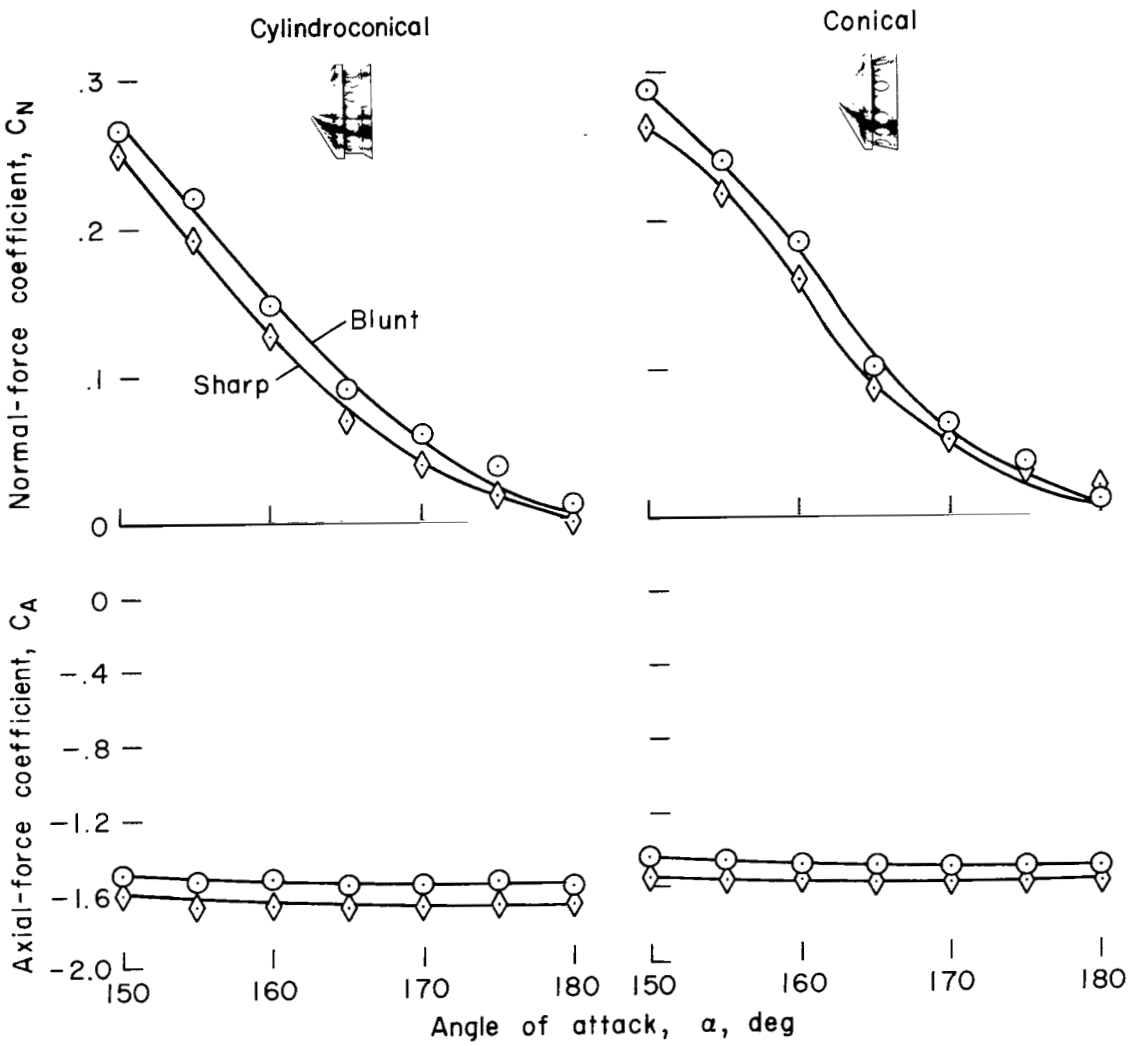

(b) Normal-force and axial-force coefficients.

Figure 12.- Concluded.

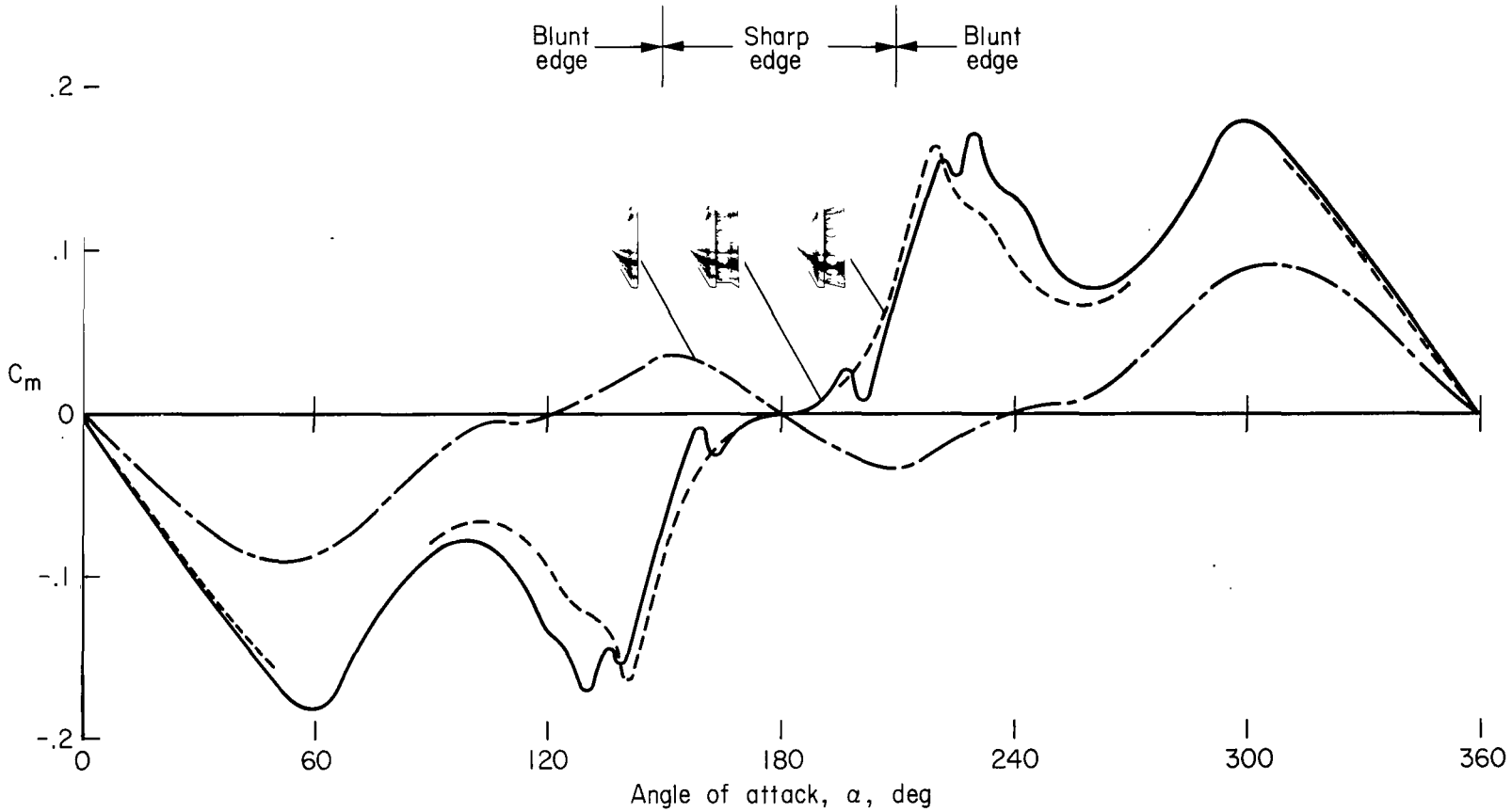

Figure 13.- Moment alterations resulting from conical and cylindroconical fences at M = 10.4.

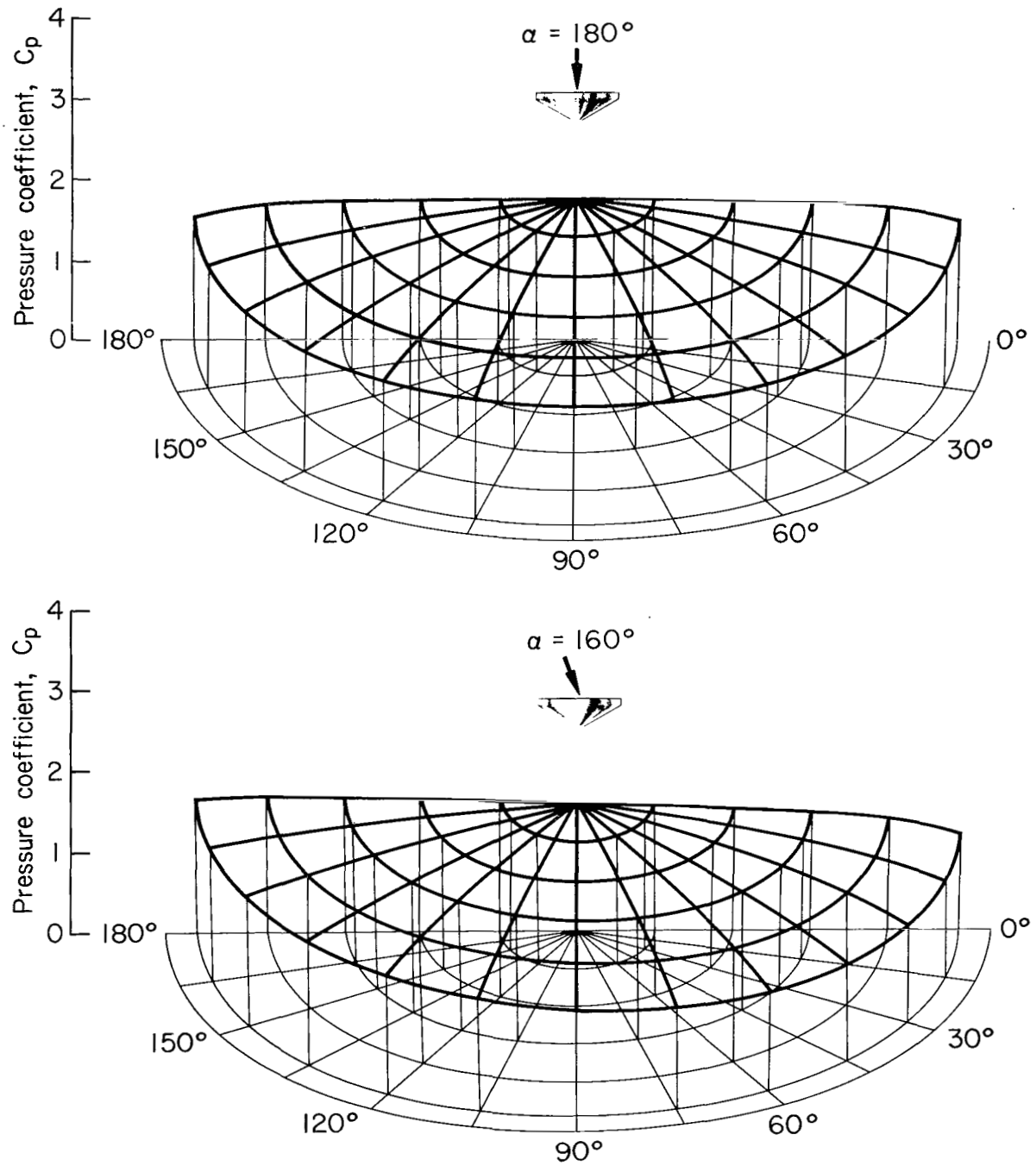

(a) No fence.

Figure 14.- Pressure distributions on the base of the sting-mounted model with and without the various blunt-edged fences, M = 10.4.

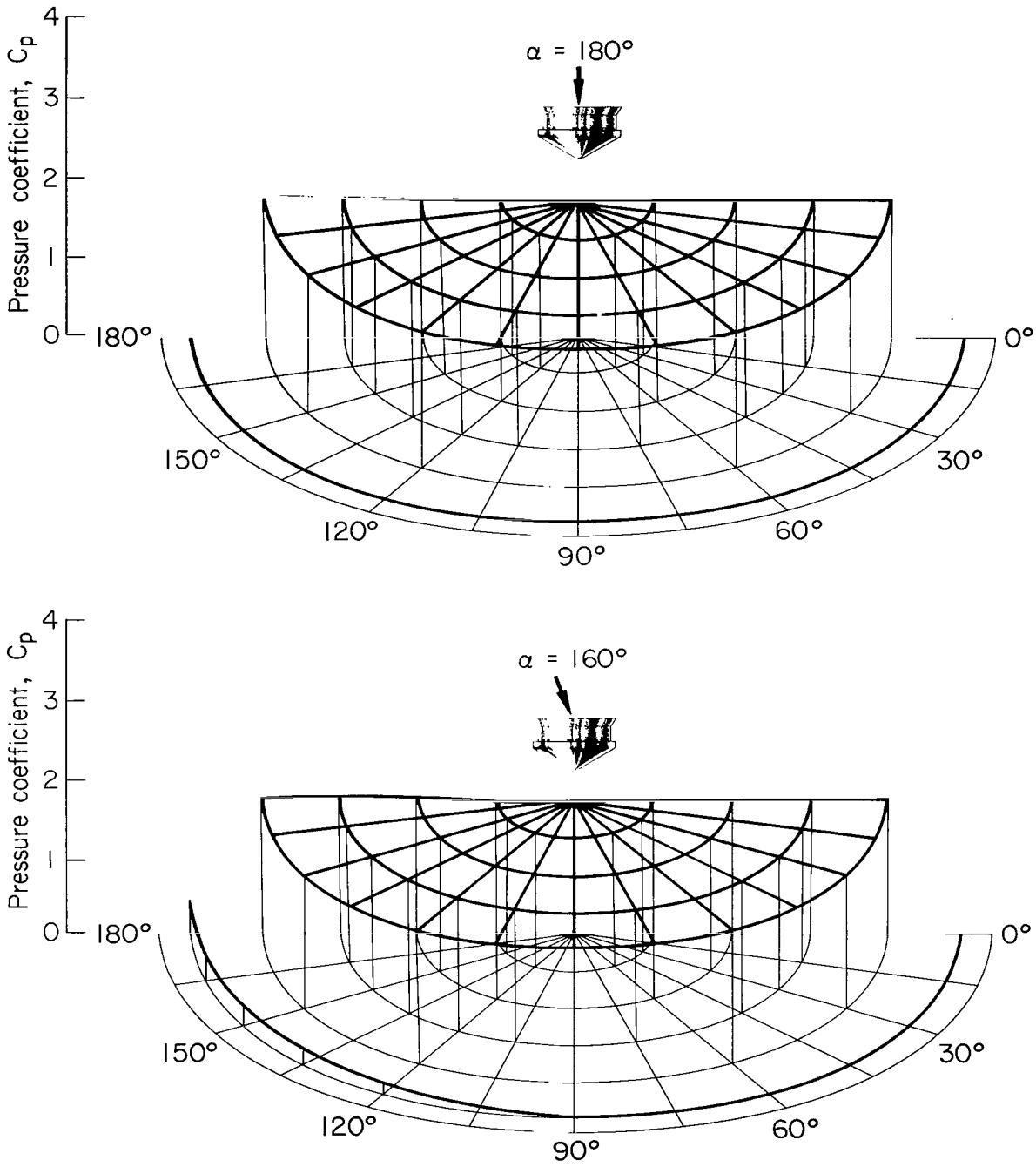

(b) Unvented cylindroconical fence.

Figure 14.- Continued.

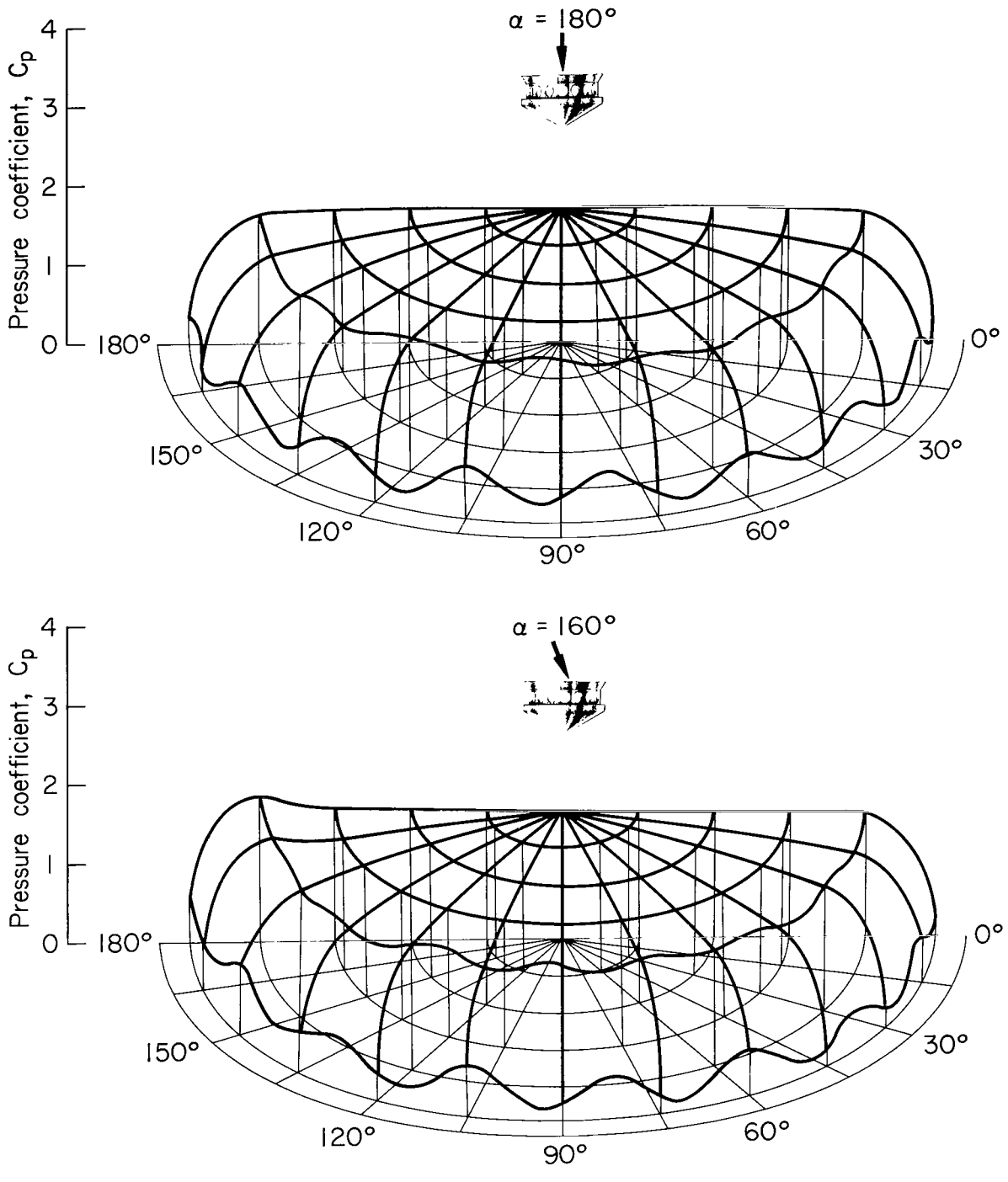

(c) Vented cylindroconical fence.

Figure 14.- Continued.

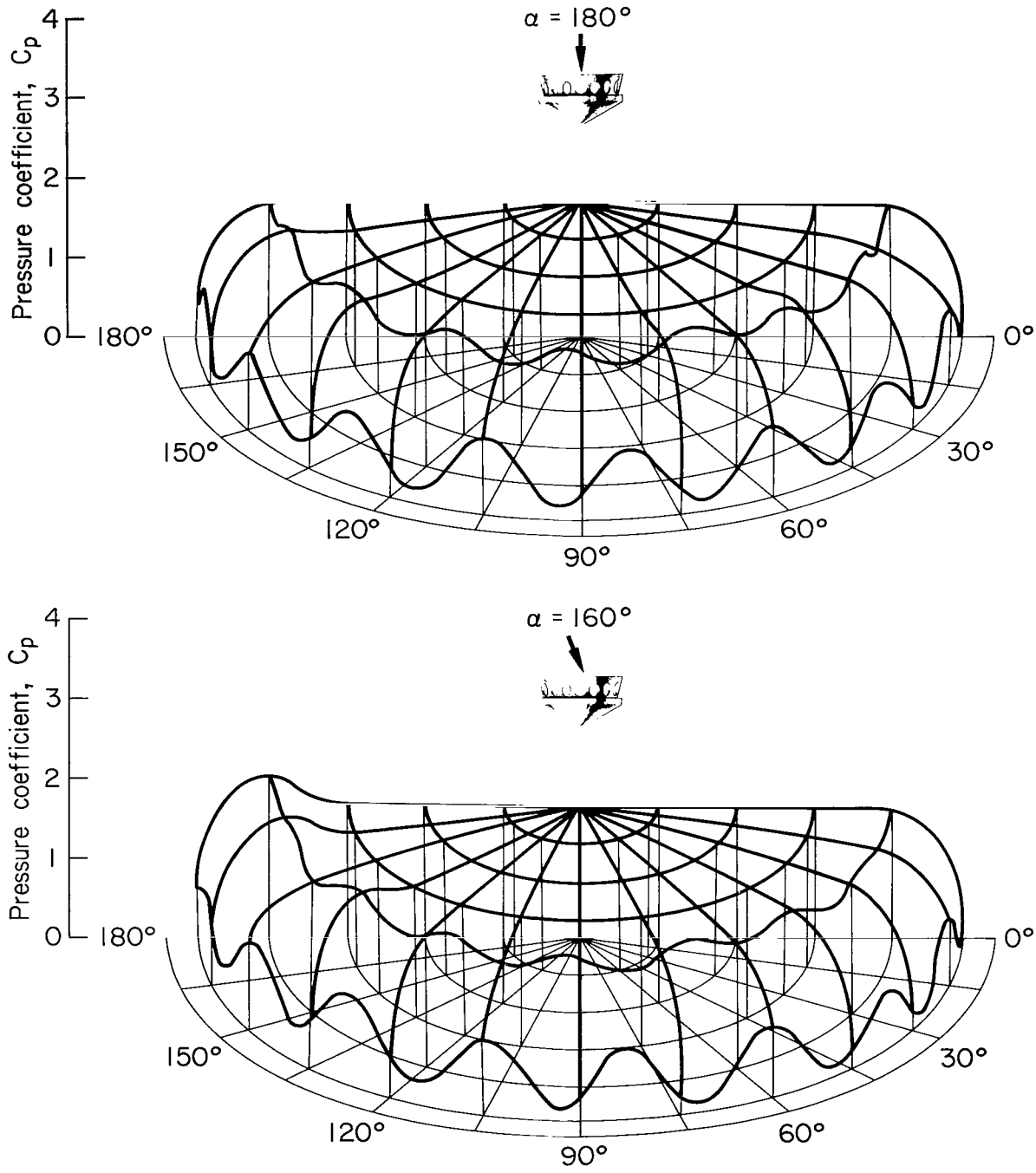

(d) Vented conical fence.

Figure 14.- Continued.

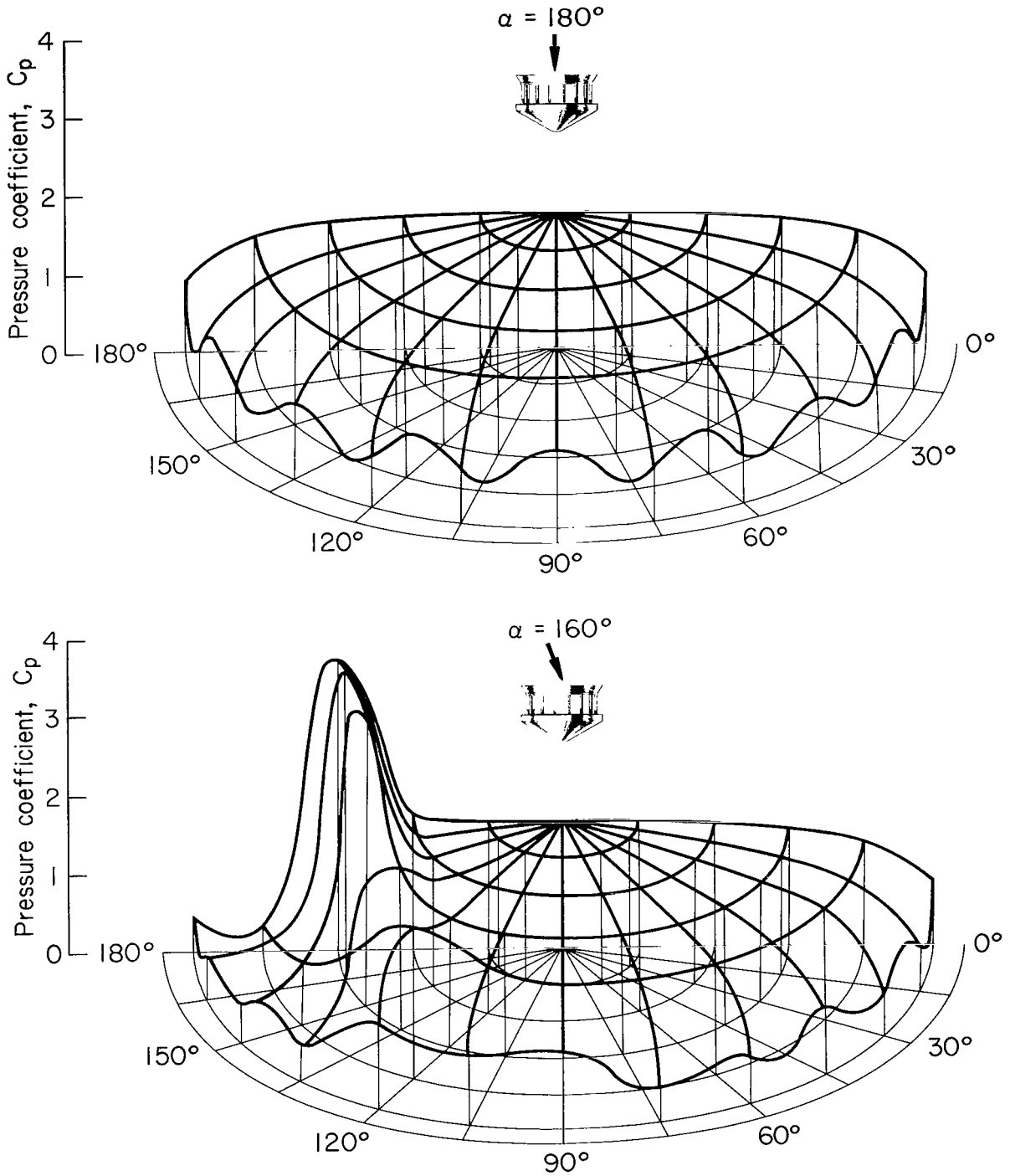

(e) Vented extended cylindroconical fence.

Figure 14.- Concluded.

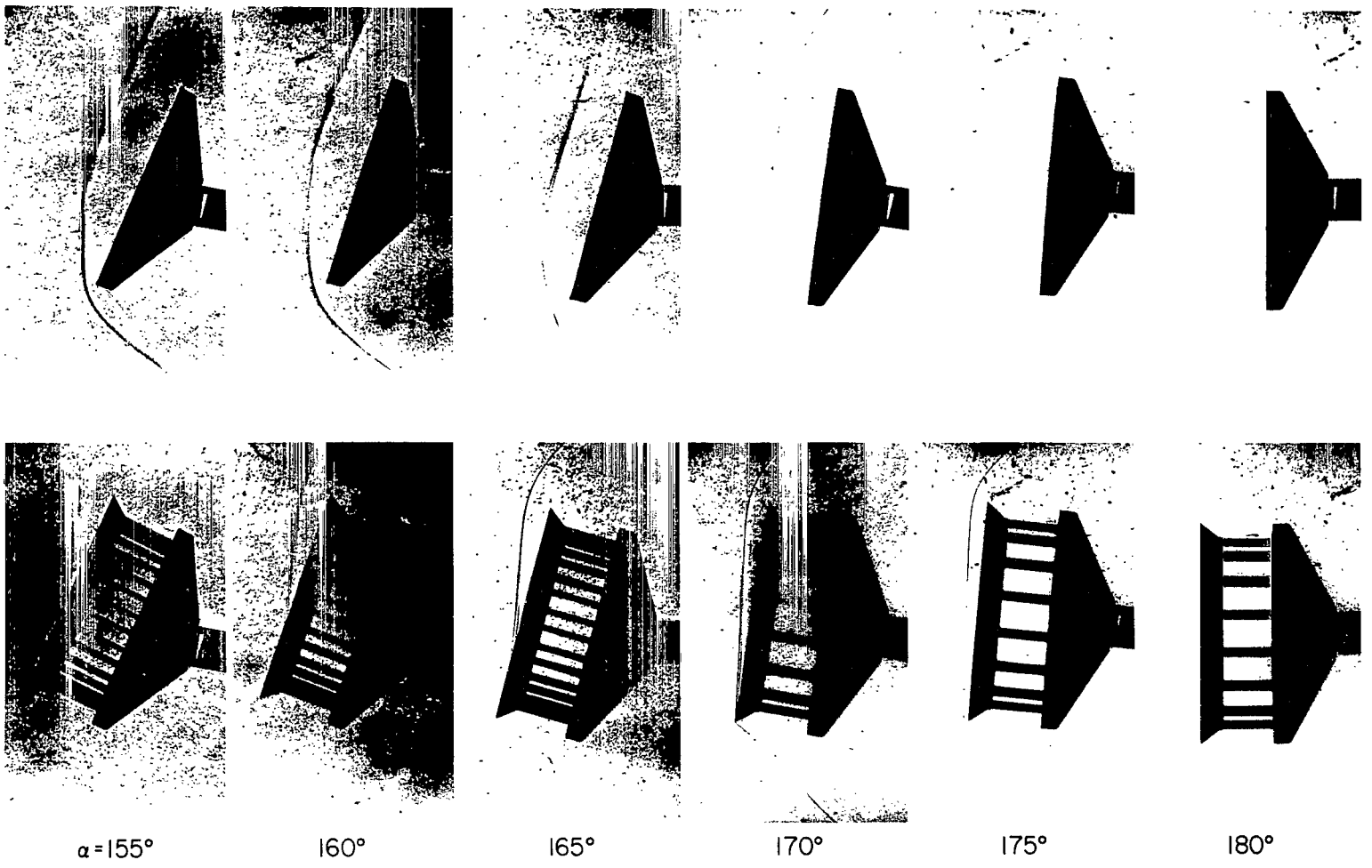

(a) Model with no fence and with extended fence.

Figure 15.- Shadowgraphs of the flow about the model with and without the various sharp-edged fences, M = 7.4.

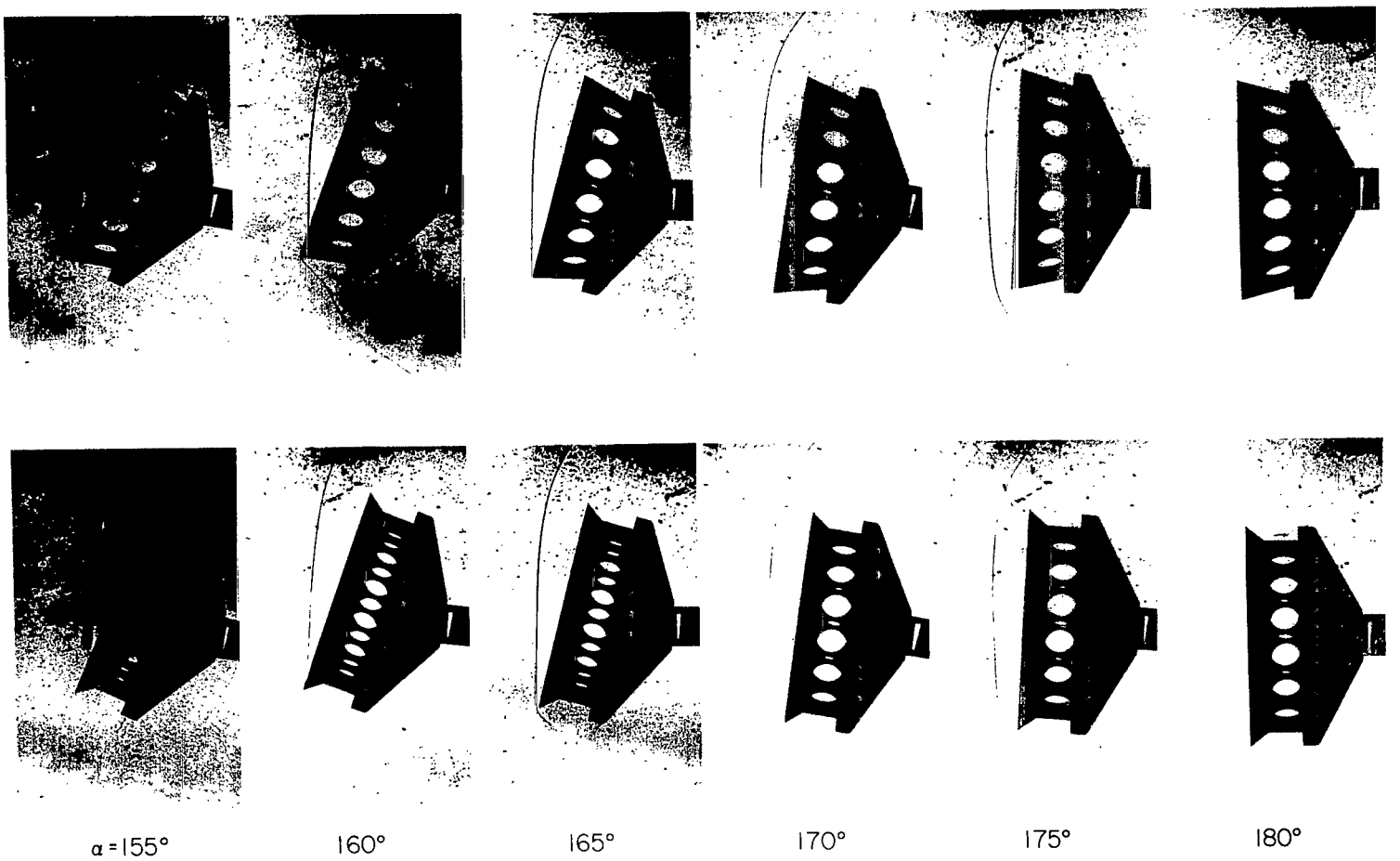

(b) Model with conical and cylindroconical fences.

Figure 15.- Concluded.

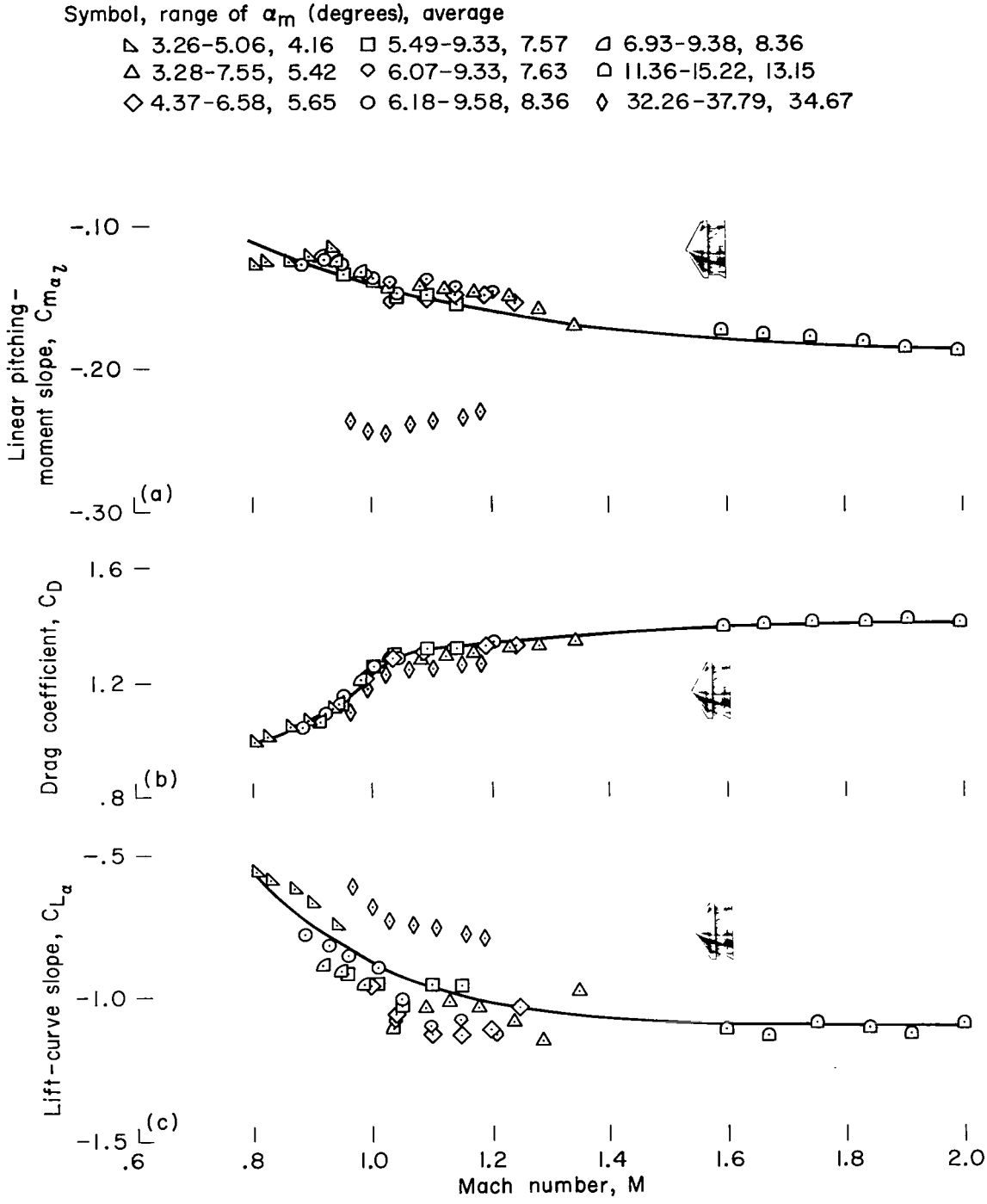

(a) Pitching-moment coefficient slope.
(b) Drag coefficient.
(c) Lift-coefficient slope.

Figure 16.- Transonic static aerodynamic characteristics, cylindroconical fence.

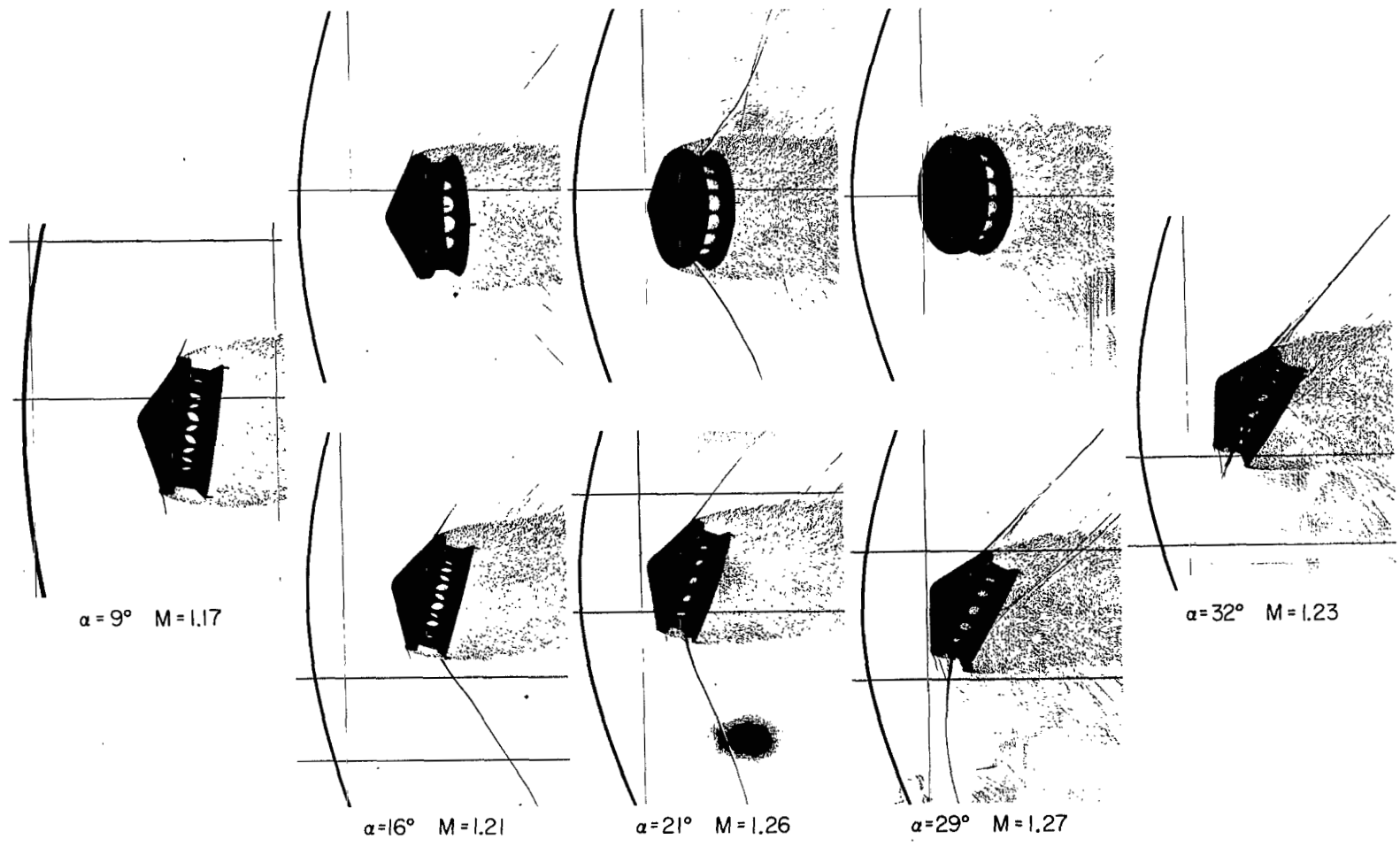

Figure 17.- Shadowgraphs illustrating shock wave development on cylindroconical fence with the model in transonic flight (vertical pairs are from orthogonal planes).

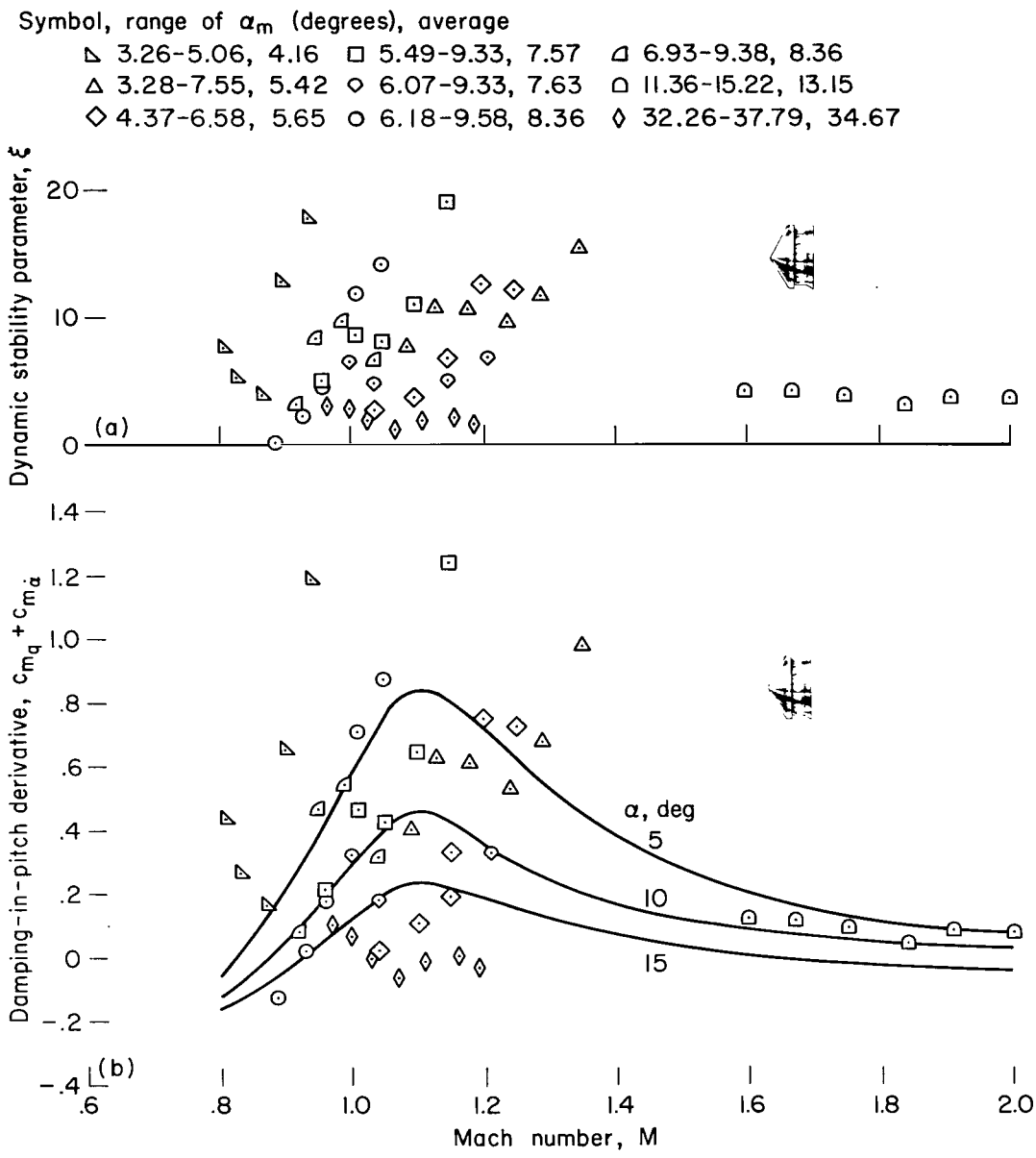

(a) Dynamic stability parameter.

(b) Damping-in-pitch derivative.

Figure 18.- Transonic dynamic aerodynamic characteristics, cylindroconical fence.

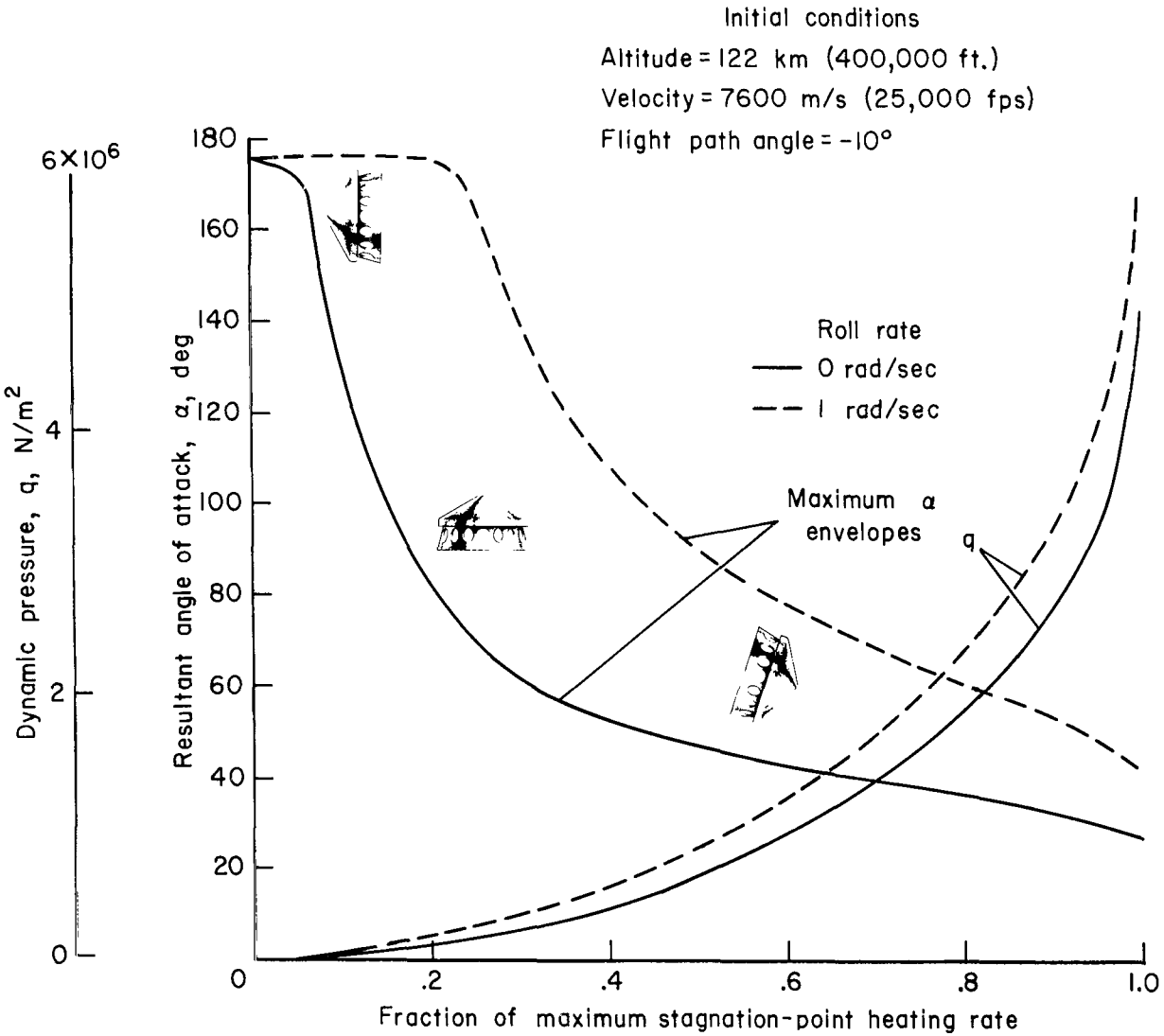

Figure 19.- Predicted motion during Earth reentry of vehicle with sharpened conical fence.

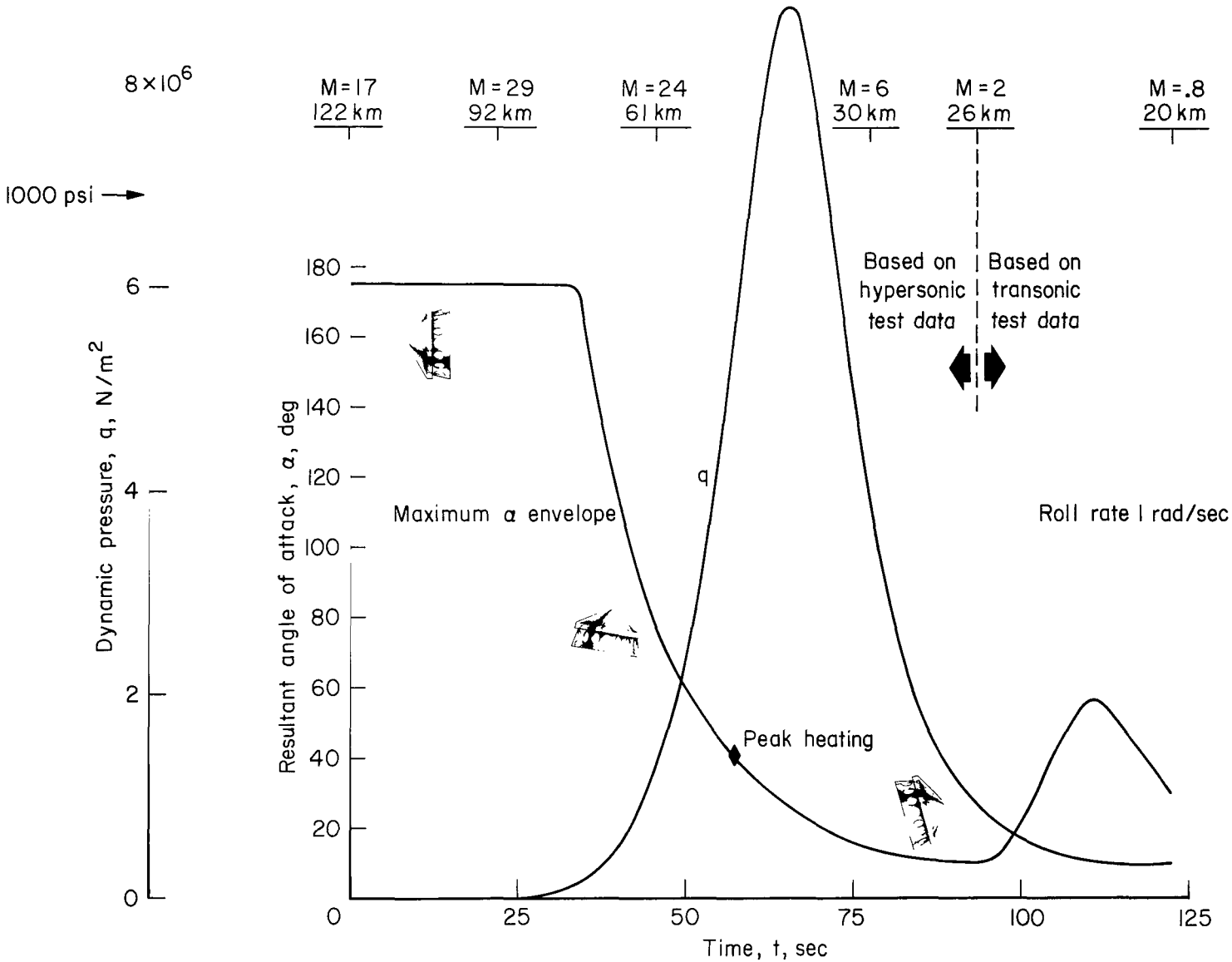

Figure 20.- Predicted motion during Earth reentry of vehicle with sharpened conical fence.

04U 001 56 51 3DS 71.10 00903
AIR FORCE WEAPONS LABORATORY /WLCL/
KIRTLAND AFB, NEW MEXICO 87117

ATT E. LOU BOWMAN, CHIEF,TECH. LIBRARY

"The aeronautical and space activities of the United States shall be conducted so as to contribute . . . to the expansion of human knowledge of phenomena in the atmosphere and space. The Administration shall provide for the widest practicable and appropriate dissemination of information concerning its activities and the results thereof."

—NATIONAL AERONAUTICS AND SPACE ACT OF 1958

NASA SCIENTIFIC AND TECHNICAL PUBLICATIONS

TECHNICAL REPORTS: Scientific and technical information considered important, complete, and a lasting contribution to existing knowledge.

TECHNICAL NOTES: Information less broad in scope but nevertheless of importance as a contribution to existing knowledge.

TECHNICAL MEMORANDUMS: Information receiving limited distribution because of preliminary data, security classification, or other reasons.

CONTRACTOR REPORTS: Scientific and technical information generated under a NASA contract or grant and considered an important contribution to existing knowledge.

TECHNICAL TRANSLATIONS: Information published in a foreign language considered to merit NASA distribution in English.

SPECIAL PUBLICATIONS: Information derived from or of value to NASA activities. Publications include conference proceedings, monographs, data compilations, handbooks, sourcebooks, and special bibliographies.

TECHNOLOGY UTILIZATION PUBLICATIONS: Information on technology used by NASA that may be of particular interest in commercial and other non-aerospace applications. Publications include Tech Briefs, Technology Utilization Reports and Technology Surveys.

Details on the availability of these publications may be obtained from:

SCIENTIFIC AND TECHNICAL INFORMATION OFFICE

NATIONAL AERONAUTICS AND SPACE ADMINISTRATION

Washington, D.C. 20546